European Journal of Medicinal Chemistry 258 (2023) 115617

Contents lists available at ScienceDirect

European Journal of Medicinal Chemistry

journal homepage: www.elsevier.com/locate/ejmech

Research paper

Antimycobacterial pyridine carboxamides: From design to *in vivo* activity

Daria Elżbieta Nawrot [a,*], Ghada Bouz [a,*], Ondřej Janďourek [a], Klára Konečná [a], Pavla Paterová [b], Pavel Bárta [a], Martin Novák [a,d], Radim Kučera [a], Júlia Zemanová [c], Martin Forbak [c], Jana Korduláková [c], Oto Pavliš [e], Pavla Kubíčková [e], Martin Doležal [a], Jan Zitko [a,*]

[a] Faculty of Pharmacy in Hradec Králové, Charles University, Heyrovského 1203, 50005, Hradec Králové, Czech Republic
[b] Department of Clinical Microbiology, University Hospital, Sokolská 581, 500 05, Hradec, Králové, Czech Republic
[c] Department of Biochemistry, Faculty of Natural Sciences, Comenius University in Bratislava, Mlynská Dolina, Ilkovičova 6, 84215, Bratislava, Slovakia
[d] Biomedical Research Center, University Hospital Hradec Kralove, Sokolská 581, 50005, Hradec Králové, Czech Republic
[e] Military Health Institute, Military Medical Agency, Tychonova 1, 160 01, Prague 6, Czech Republic

ARTICLE INFO

Keywords:
4-Aminosalicylic acid
Isoniazid
Multidrug-resistance
Pyrazinamide
Pyridine
Tuberculosis

ABSTRACT

Tuberculosis is the number one killer of infectious diseases caused by a single microbe, namely *Mycobacterium tuberculosis (Mtb)*. The success rate of curing this infection is decreasing due to emerging antimicrobial resistance. Therefore, novel treatments are urgently needed. As an attempt to develop new antituberculars effective against both drugs-sensitive and drug-resistant *Mtb*, we report the synthesis of a novel series inspired by combining fragments from the first-line agents isoniazid and pyrazinamide (series I) and isoniazid with the second-line agent 4-aminosalicylic acid (series II). We identified compound **10c** from series II with selective, potent *in vitro* antimycobacterial activity against both drug-sensitive and drug-resistant *Mtb* H37Rv strains with no *in vitro* or *in vivo* cytotoxicity. In the murine model of tuberculosis, compound **10c** caused a statistically significant decrease in colony-forming units (CFU) in spleen. Despite having a 4-aminosalicylic acid fragment in its structure, biochemical studies showed that compound **10c** does not directly affect the folate pathway but rather methionine metabolism. *In silico* simulations indicated the possibility of binding to mycobacterial methionine-tRNA synthetase. Metabolic study in human liver microsomes revealed that compound **10c** does not have any known toxic metabolites and has a half-life of 630 min, overcoming the main drawbacks of isoniazid (toxic metabolites) and 4-aminosalicylic acid (short half-life).

1. Introduction

The difficult times people worldwide had to experience with the COVID-19 pandemic made us realize how unprepared we are to face infections. This fact triggers particularly medicinal chemists as the first players in drug development to design and prepare antimicrobial agents for various infections, especially those that we are already fully aware of their seriousness and the lack of proper treatment. Beside viral infections, bacterial infections are growing every day as a real challenge costing people their lives. One example of a highly contagious, hard-to-treat bacterial infection is tuberculosis (TB). In fact, TB is the leading cause of death from a single infectious agent according to the World Health Organization (WHO) [1]. Global mobilization today has ended the stereotype that TB is a third-world country disease. First-line antitubercular agents are isoniazid (INH), pyrazinamide (PZA), rifampicin (RIF), and ethambutol (EMB), while second-line antituberculars include agents that are either less active or preserved for drug-resistant cases, such as streptomycin (STM), fluoroquinolones, bedaquiline, and 4-aminosalicylic acid (PAS), among others. Beside the complex, lengthy treatment to manage drug-sensitive cases, multidrug-resistant TB (MDR-TB) and extensive drug-resistant TB (XDR-TB) are increasing in number, during which patients are left on palliative care [1].

In continuation of previous efforts to prepare new agents with promising antitubercular activity, we present the design, synthesis, and biological evaluation of a series of pyridine carboxamides. Nitrogen containing heterocycles play vital roles in many divisions of medicinal

* Corresponding authors. Faculty of Pharmacy in Hradec Králové, Charles University, Heyrovského 1203, Hradec Králové, 500 05, Czech Republic.
E-mail addresses: nawrotd@faf.cuni.cz (D.E. Nawrot), bouzg@faf.cuni.cz (G. Bouz), jando6aa@faf.cuni.cz (O. Janďourek), konecna@faf.cuni.cz (K. Konečná), pavla.paterova@fnhk.cz (P. Paterová), bartp7aa@faf.cuni.cz (P. Bárta), martin.novak@fnhk.cz (M. Novák), kucerar@faf.cuni.cz (R. Kučera), julia.zemanova@uniba.sk (J. Zemanová), forbak1@uniba.sk (M. Forbak), jana.kordulakova@uniba.sk (J. Korduláková), oto.pavlis@email.cz (O. Pavliš), pafcule@centrum.cz (P. Kubíčková), dolezalm@faf.cuni.cz (M. Doležal), jan.zitko@faf.cuni.cz (J. Zitko).

https://doi.org/10.1016/j.ejmech.2023.115617
Received 24 April 2023; Received in revised form 29 June 2023; Accepted 29 June 2023
Available online 30 June 2023

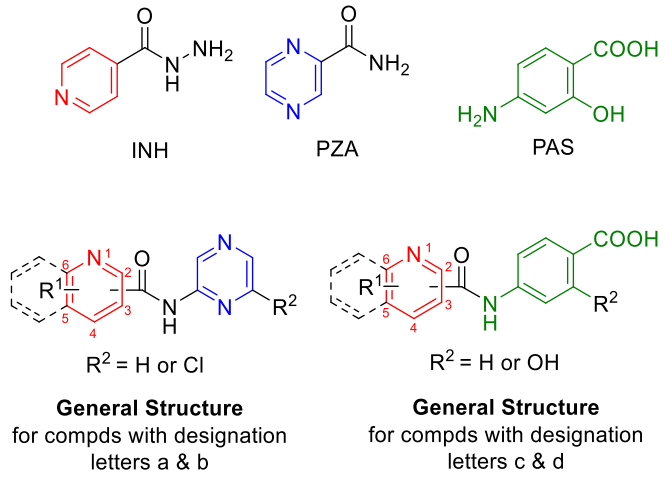

Fig. 1. Design Rationale. The chemical structures of INH; PZA; PAS; general structures of title compounds. For R^1 and R^2 refer to Table 1.

chemistry, especially as anti-infectives [2–4]. The series is subdivided into two main general structures; for compounds with designation letters **a** & **b**, pyridine carboxylic acids were linked to aminopyrazine (AP), or 6-chloropyrazin-2-amine (6-Cl-AP) via an amidic bond – total 16 compounds; for compounds with designation letters **c** & **d**, pyridine carboxylic acids were linked to PAS, or 4-aminobenzoic acid (PABA) via an amidic bond – total 16 compounds, refer to Fig. 1 for general structures. The design can be justified as an attempt to combine the first line INH (which is a hydrazide of isonicotinic acid and hence the pyridine core) with the core of PZA (general structure for compounds with designation letters **a** & **b**) and PAS (general structure for compounds with designation letters **c** & **d**). In the Supplementary Data a coding guide of final compounds is enclosed. INH exerts its antimycobacterial activity by inhibiting the synthesis of mycolic acids in mycobacteria [5]. The ambiguity of PZA's mode of action and the multi-target theory make it rational from a medicinal chemistry point of view to prepare various derivatives against different targets [6]. PAS on the other hand targets (after activation) mycobacterial dihydrofolate reductase (DHFR) [7]. The main drawback of INH is the formation of the hepatotoxic metabolites hydrazine and acetyl-hydrazine [8], while drawbacks of PAS include short half-life and rapid clearance that requires the administration of large doses and hence unpleasant gastrointestinal side effects [9].

Final compounds were *in vitro* screened against slow-growing mycobacterial strains [*Mycobacterium tuberculosis* H37Rv (*Mtb* H37Rv), *Mycobacterium tuberculosis* H37Ra (*Mtb* H37Ra), *Mycobacterium kansasii* (*M. kansasii*), *Mycobacterium avium* (*M. avium*)], fast-growing mycobacterial strains *Mycolicibacterium smegmatis* (*M. smegmatis*), *Mycolicibacterium aurum* (*M. aurum*)] and for their *in vitro* cytotoxicity on Hep G2 liver cancer cell line. As complementary testing, compounds were also screened for *in vitro* antibacterial and antifungal activities against pathogens of clinical importance. The most promising compounds were further advanced for *in vitro* antimycobacterial activity screening against MDR *Mtb*, a metabolic study in human liver microsomes, along with *in vivo* toxicity evaluation in *Galleria mellonella* and *in vivo* antimycobacterial efficacy evaluation in a murine model of TB. The mechanism of action of the most active compound was also investigated by biochemical and *in silico* studies.

2. Results and discussion

2.1. Chemistry

All final compounds were prepared by a simple coupling between the corresponding starting pyridine carboxylic acid and the amino-bearing fragment (AP, 6-Cl-AP, PAS, PABA). The acids were activated by CDI or oxalyl chloride, and final compounds precipitated upon the addition of diluted hydrochloric acid (5% HCl). The precipitate was filtered off and recrystallized from water. The final compound with δ-lactone (compound **10c'**) was synthesized by preparing the lactone of PAS first and then reacting it with quinaldic acid. Cyclization was achieved using potassium phosphate tribasic, DCM, and DMF, heating to 100 °C under a condenser for 10 h (Scheme 1). The reaction mixture was recharged with DCM every 3 h. The reaction was monitored by TLC (mobile phase hexane in ethyl acetate 1:1), and upon completion, the mixture was extracted in DCM/water, according to the procedure reported in Ref. [10], and purified by flash chromatography using gradient elution from 0 to 100% ethyl acetate in hexane.

In total, we prepared 37 compounds isolated as solids and characterized by ^{1}H NMR and ^{13}C NMR spectra, elemental analysis and IR spectra. Obtained data were consistent with the proposed structures. In the ^{1}H NMR spectra (DMSO-d_6), the amidic proton was observed at 11.77–10.41 ppm for series **a**, at 12.05–10.78 ppm for series **b**, at 11.63–10.59 ppm for series **c** and at 11.00–10.66 ppm for series **d**.

2.2. Biological activity evaluation

A literature search revealed that compounds **1c** and **2c** were fragments of larger structures evaluated as potential antituberculars; however, they were not evaluated themselves [11]. Besides, compound **1a** was evaluated as a compound for altering the life span of eukaryotes [12], and **5a** was evaluated as an activator of caspase and hence an inducer of apoptosis [13]. Compound **10d** was assessed as an inhibitor of protein synthesis that inactivates certain toxins [14] and as a methionyl-tRNA synthetase inhibitor [15]. The latter is of greater importance for our work since aminoacyl-tRNA synthetases are gaining more interest as targets for antitubercular drug discovery [16]. All prepared compounds passed PAINS and Aggregators screening using ZINC15 utility (http://zinc15.docking.org/patterns/home; accessed in June 2022).

2.2.1. Antimycobacterial activity evaluation

Final compounds were evaluated for their *in vitro* antimycobacterial activity against six mycobacterial strains; *Mtb* H37Rv, *Mtb* H37Ra, *M. kansasii*, *M. avium*, *M. smegmatis*, and *M. aurum* using a Microplate Alamar Blue Assay [17]. *Mtb* H37Ra is a surrogate strain to the highly pathogenic strain *Mtb* H37Rv, and according to the literature, MIC values against the two strains are qualitatively comparable [18]. *M. kansasii* and *M. avium* are two pathogenic slow-growing mycobacteria causing so-called mycobacterioses with rapidly increasing clinical importance, while *M. smegmatis* and *M. aurum* are non-tubercular,

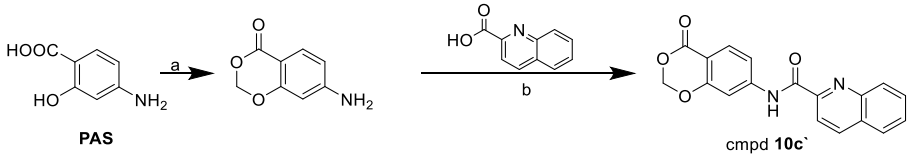

Scheme 1. Synthetic routes for compound **10c'**. a) $K_3PO_4.3H_2O$, DCM, DMF, 100 °C, reflux, 10 h; b) CDI, DCM, overnight, RT.

fast-growing mycobacteria that cause opportunistic infections in immunocompromised patients [19]. We also evaluated the *in vitro* antimycobacterial activity of the starting pyridine carboxylic acids and when activity was detected against *Mtb* H37Rv, their corresponding primary amides were prepared and evaluated as well. The active pyridine carboxylic acids were 2-picolinic acid (MIC = 6.25 μg/mL; 50.77 μM), 4-methoxypyridine-2-carboxylic acid (12.5 μg/mL; 81.62 μM), and quinaldic acid (12.5 μg/mL; 72.18 μM). It must be noted that all of the three corresponding amides, namely picolinamide, 4-methoxypicolinamide, and quinoline-2-carboxamide, were inactive. Results are summarized in Table 1.

When we want to compare series we find that series **a** and **b**, based on pyrazine core, were completely inactive, series **d**, based on PABA, had low activity while all compounds in series **c**, based on PASA, possessed good antimycobacterial activity.

The nature of the substituent (R^1) and the pyridine acid (position of the N atom in the aromatic ring) had no influence on the detected antimycobacterial activity, highlighting the significant role of the PAS fragment. Exceptions are compounds **7a** and **7b** (both of which bear CF_3 substituent) which were active against *M. kansasii* (MIC = 6.25 μg/mL). The introduction of chlorine atom on pyridine ring (R^2) in series b (**1b**–**5b**, **6b**, **10b**) did not improve the antimycobacterial activity despite the increase in lipophilicity.

From the PABA series (**2d**, **5**–**7d**, **10d**) we can conclude the importance of the hydroxyl group at position 2 of the phenyl ring of PAS; when comparing matching pairs between the **c** and **d** series, we find that every time compounds **d** have inferior activity. The most active among all is compound **10d** (highlighting the significance of quinaldic moiety).

As we mentioned earlier, we have evaluated the starting pyridine carboxylic acids for their *in vitro* antimycobacterial activity. Among all, only 2-picolinic acid, 4-methoxypyridine-2-carboxylic acid, and quinaldic acid exerted some antimycobacterial activity against *Mtb* H37Rv and hence we prepared and evaluated their corresponding amides. We found that the amides lost their activity. It must be noted that quinaldic acid has documented antimicrobial activity in the literature [21].

Regarding antimycobacterial activity against the remaining mycobacterial strains, compounds bearing CF_3 substituent (**7a**, **7b**, **7c**), **5c** and **10d** exerted activity against *M. kansasii* comparable to INH; only compounds **7c** and **10d** exerted activity against *M. avium* comparable to INH; only compounds **2c** and **10c** exerted activity against *M. smegmatis* comparable to INH; none of the title compounds had significant activity against *M. aurum*.

It can be concluded from Table 1 that compounds **7c** and **10c** are the most broad-spectrum compounds. The most active compound against the virulent strain *Mtb* H37Rv was compound **10c** (MIC = 5.06 μM), hence we prepared a δ-lactone prodrug (**10c′**) as an attempt to increase lipophilicity and subsequently facilitate penetrating the thick mycobacterial cell wall. The lactone had a positive effect solely on antimycobacterial activity against *Mtb* H37Ra. Compounds **10c** and its lactone **10c′** were evaluated against two multi-drug resistant (MDR-TB) strains (refer to Table 2 for results and resistance patterns). MDR-TB is defined as resistance to both INH and RIF [22]. *In vitro* activity was determined according to details mentioned in section 1.2 in Supplementary Data. The complete resistance profile of MDR *Mtb* strains can be found in Table S1 in Supplementary Data. Compound **10c** retained its antimycobacterial activity against MDR strains, while its lactone form was not able to. Compound **10c** and its lactone **10c′** were advanced into further investigations mentioned in the following sections.

2.2.2. Antibacterial and antifungal activity evaluation

Microdilution broth method was performed according to EUCAST recommendations [23–25], with slight modifications. None of the tested compounds exerted neither antibacterial (against *Staphylococcus aureus*, methicillin-resistant *Staphylococcus aureus*, *Staphylococcus epidermidis*, *Enterococcus faecalis*, *Escherichia coli*, *Klebsiella pneumoniae*, *Acinetobacter baumannii*, *Pseudomonas aeruginosa)* nor antifungal (against *Candida albicans*, *Candida krusei*, *Candida parapsilosis*, *Candida tropicalis*, *Aspergillus fumigatus*, *Aspergillus flavus*, *Lichtheimia corymbifera*, *Trichophyton interdigitale*) activity up to the highest tested concentration of 500 μM, refer to Table S2 and Table S3, respectively, in Supplementary Data for MIC values of standards.

2.2.3. Cytotoxicity evaluation

In vitro model of human hepatocellular carcinoma (Hep G2) cell line was used to assess the cytotoxicity of title compounds. This model is routinely used in the literature for *in vitro* cytotoxicity evaluation, however, in our case, it is of greater value since the multi-drug *anti*-TB regimen is known to carry an augmented risk of hepatotoxicity. Results are presented as the inhibitory concentration that reduces the viability of the cell population to 50% of the maximum viability (IC_{50}) in Table 1. No significant cytotoxicity was detected for title compounds except for the compounds bearing $–CF_3$ substituent, regardless of the structural type (IC_{50} for **7a** = 145.9 μM, **7b** = 209 μM, **7c** = 163.1 μM, **7d** = 248 μM). The high toxicity of such compounds makes their detected antimycobacterial activity non-selective.

2.3. Advanced testing for compound *10c* and its lactone compound *10c′*

2.3.1. In vivo toxicity evaluation using Galleria mellonella animal model

In order to determine the toxicity of compound **10c** *in vivo*, the invertebrate animal model, *Galleria mellonella*, was employed [26]. The lactone form was excluded from evaluation due to poor water solubility. The toxicity of compound **10c** was evaluated after two ways of drug administration, via intrahemocoel and peroral. Animals were divided into groups according to the final amount of administered compound per kg of body weight. Final administered doses approximately corresponded to the recommendation of Organization for Economic Co-operation and Development (OECD) test guidelines for chemicals [26]. After administration, the mortality of larvae was monitored for five days. See section 5 in Supplementary Data for full methodology and results (Tables S4 and S5). In conclusion, compound **10c** could be categorized into class 4 according to the Globally Harmonised System (GHS) that represents non-toxic, or very low toxic compounds.

2.3.2. In vivo antimycobacterial activity evaluation in a murine model of TB

In vivo antimycobacterial activity of the PAS fragment-containing compounds **10c** and **5c** (with best *in vitro* antimycobacterial activity against *Mtb* H37Rv, refer to Table 1) was determined in a murine model of TB infection. To improve the water solubility, for the administration, the compounds were tested in the form of a sodium salt (**10cNa**), or sodium salt dihydrate (**5cNa.2H$_2$0**). The mice were infected intranasally with *Mtb* H37Rv and the infection was let to develop for four weeks. After this initialization period (day 0), the mice were treated with the test compounds for 28 days. Compounds were administered as a water solution by force-feeding (gastric tube). After the experiment, the CFU values were determined in lungs and spleen and compared to the untreated control group (Fig. 2). The results in lungs were ambiguous and with none or low statistical significance. More robust results were observed in the spleen, where both **10c** and **5c** caused a statistically significant reduction of CFU.

2.3.3. Determination of the mechanism of action

2.3.3.1. Determination of the MIC of compound 10c against Mtb H37Ra overproducing enzymes of the folate pathway. Since PAS is an important part of the structure of compound **10c**, we were interested to know whether **10c** exhibits the same mechanism of antimycobacterial action as PAS. It was shown that PAS is recognized by dihydropteroate synthase FolP1 (Rv3608c) as its natural substrate 4-aminobenzoic acid [7]. The product of this reaction is further metabolized by dihydrofolate synthase

Table 1
Prepared compounds with their calculated lipophilicity (log *P*, ChemDraw v20.0.), antimycobacterial activity expressed as minimum inhibitory concentration (MIC), and human hepatocellular carcinoma cell (Hep G2) cytotoxicity expressed as half maximal inhibitory concentration (IC_{50}).

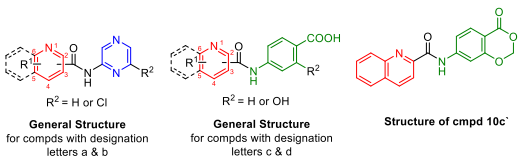

Code	Positional isomer[a]	R^1	R^2	Log *P*	Antimycobacterial Activity MIC in μg/mL (μM)						Hep G2 IC_{50} (μM)	SI[e]
					Mtb H37Rv	*Mtb* H37Ra	*M. kansasii*	*M. avium*	*M. smeg.*	*M. aurum*		
AP	–	–	–	−0.73	>100	≥500	>100	>100	≥500	≥500	>1000	
1a	4	H	H	−0.46	>100	≥500	>100	>100	≥500	≥500	>1000	
2a	2	H	H	−0.03	>100	250	>100	>100	≥500	≥500	>1000	
3a	2	4-OCH_3	H	−0.16	>100	≥250	50	>100	≥250	≥250	>250[d]	
4a	4	2-CH_3	H	0.25	>100	≥250	>100	>100	≥250	≥250	>1000	
5a	3	6-Cl	H	0.45	>100	≥250	>100	>100	≥250	≥250	>1000	
6a	2	6-Cl	H	0.87	>100	≥500	50	>100	≥500	≥500	>250[d]	
7a	2	5-CF_3	H	0.89	50	≥500	6.25	>100	≥500	≥500	145.9	
9a	4	2-Cl, 6-CH_3	H	1.15	>100	≥500	>100	>100	≥500	≥500	>250[d]	
10a	2[b]	–	H	1.39	>100	≥125	>100	>100	≥125	≥125	>100[d]	
6-Cl- AP	–	–	–	0.17	>100	≥500	>100	>100	≥500	≥500	>1000	
1b	4	H	Cl	0.45	>100	≥500	>100	>100	≥500	≥500	>1000	
2b	2	H	Cl	0.87	>100	≥250	>100	>100	≥250	≥250	>100[d]	
3b	2	4-OCH_3	Cl	0.74	>100	≥500	>100	>100	≥500	250	>500[d]	
4b	4	2-CH_3	Cl	1.15	>100	≥500	>100	>100	≥500	250	>1000	
5b	3	6-Cl	Cl	1.35	100	≥500	>100	>100	≥500	≥500	>500[d]	
7b	2	5-CF_3	Cl	1.79	100	≥250	6.25	>100	≥250	≥250	209	
10b	2[b]	–	Cl	2.29	>25	≥125	>25	>25	≥125	≥125	>25[d]	
PAS	–	–	–	0.40	3.13 (20.44)	0.25	n.a.	3.13	500	250	1270 [20]	62.1
1c	4	H	OH	0.67	3.13 (12.12)	≥125	50	100	≥125	≥125	>1000	82.5
2c	2	H	OH	1.09	1.56 (6.04)	250	50	>100	15.625	62.5	>1000	165.5
3c	2	4-OCH_3	OH	0.97	1.56 (5.41)	31.25	>100	>100	125	62.5	>1000	184.8
4c	4	2-CH_3	OH	1.37	12.5 (45.91)	≥125	>100	>100	≥125	≥125	>1000	21.8
5c	3	6-Cl	OH	1.57	1.56 (5.33)	125	12.5	100	≥250	≥250	>1000	187.6
6c	2	6-Cl	OH	1.99	3.13 (10.69)	125	>100	>100	125	125	>1000	93.5
7c	2	5-CF_3	OH	2.01	3.13 (9.59)	31.25	12.5	12.5	250	62.5	163.1	34.1
8c	4	2-OH, 6-CH_3	OH	1.7	6.25 (21.68)	≥500	>100	>100	≥500	≥500	>1000	46.1
9c	4	2-Cl, 6-CH_3	OH	2.28	50	250	>100	>100	≥500	≥500	>1000	
10c	2[b]	–	OH	2.51	1.56 (5.06)	31.25	100	100	31.25	15.625	>1000	197.6
10c'	2[b]	–	–	3.07	1.56 (4.87)	1.98	>100	>100	≥250	≥250	>25[d]	>5.1
PABA	–	–	–	0.79	>100	250	>100	>100	≥500	250	>1000	
2d	2	H	H	1.48	>100	125	>100	>100	≥500	250	>250[d]	
5d	3	6-Cl	H	1.96	>100	62.5	>100	>100	≥500	250	>250[d]	
6d	2	6-Cl	H	2.38	>100	62.5	>100	>100	≥500	250	>250[d]	
7d	2	5-CF_3	H	2.4	50	62.5	50	>100	≥500	62.5	248	
10d	2[b]	–	H	2.9	25 (85.53)	31.25	25	25	≥500	62.5	>50[d]	>0.6
PZA	–	–	–	−1.31	>100[c]	≥500	>100	>100	≥500	≥500	>1000	
INH	–	–	–	−0.64	0.2	0.25	12.5	12.5	15.625	3.91	>1000	
RIF	–	–	–	4.24	n.a.	0.003	n.a.	n.a.	12.5	0.198	>500[d]	
CIP	–	–	–	1.32	n.a.	0.25	n.a.	n.a.	0.125	0.016	>500[d]	

n. a. = not available.
[a] Identifies the position of the carboxyl moiety on the pyridine ring (or quinoline ring for compounds 10a, 10b and 10c).
[b] A derivative of quinaldic acid (quinoxaline-2-carboxylic acid).
[c] MIC value from testing at pH = 5.6 (acidic) is 6.25–12.5 μg/mL. The value stated in the table is from testing at pH = 6.6 (neutral).
[d] Measurements at higher concentrations were not possible due to the precipitation of the tested compound in the cell culture medium.
[e] Selectivity index (SI) = IC_{50} (μM)/$MIC_{Mtb\ H37Rv}$ (μM) calculated for active compounds having $MIC_{Mtb\ H37Rv} \leq 25$ μg/mL

Table 2
MIC values in μg/mL of compounds **10c** and **10c'** against MDR-TB.

MIC in μg/mL			
Cmpd.	*Mtb* H37Rv	*Mtb* IZAK	*Mtb* MATI
10c	1.56	6.25	12.5
10c'	1.56	50	50

Resistance patterns.
Mtb H37Rv virulent, drug-sensitive strain.
Mtb IZAK resistant to INH, RIF, STM.
Mtb MATI resistant to PZA, INH, RIF, STM.

FolC (Rv2447c) to hydroxyl dihydrofolate antimetabolite, which inhibits dihydrofolate reductases DfrA (Rv2673c) or RibD (Rv2671) [27]. To evaluate the effect of the studied compound on the folate pathway, we determined the MIC of compound **10c**, as well as its sodium salt **10cNa** against *M. tuberculosis* H37Ra mutants overproducing proteins FolP1, FolC, DfrA or RibD, respectively. We observed that the sensitivity of all tested overproducing strains against compound **10c** or its sodium salt was comparable to the sensitivity of control strains carrying an empty vector (Table 3). These data indicate that compound **10c** does not target the dihydrofolate pathway in mycobacteria.

2.3.3.2. The effect of 10c on lipids and mycolic acids. In order to clarify the mode of action of **10c** in mycobacteria we performed ^{14}C metabolic labeling of *Mtb* H37Rv cells treated with different concentrations of this compound. As specific changes in lipid profile might suggest an inhibition of some vulnerable targets (f. e. DprE1/2 [28], EmbC/B [29], InhA [30], HadA [31]), we focused on the analysis of the effect of **10c** on ^{14}C labeled lipids and mycolic acids. The cells *Mtb* H37Rv were treated with 0, 1.5, 3 or 6 μg/ml compound **10c**, or its sodium salt, for 24 h, then ^{14}C acetate was added to the culture media and the cells were cultivated for further 24 h. TLC analysis of ^{14}C labeled lipids did not reveal any significant changes in the production of major phospholipids, as well as in the production of trehalose monomycolates and trehalose dimycolates, which would suggest that **10c** causes disruption of the membrane, inhibition of cell wall synthesis, or inhibition of mycolic acids production (Fig. 3A). Treatment with **10c** led to decreased synthesis of triacylglycerols, however this phenomenon should not be lethal for mycobacteria. Interestingly, TLC analysis of fatty/mycolic acids derivatized to corresponding methyl esters revealed that **10c** affects the synthesis of methoxy- and cyclopropyl-mycolic acids, leading to the accumulation of unsaturated forms of mycolates (Fig. 3). This observation indicates that **10c** might affect the activity of methyltransferases catalyzing those steps or the levels of S-adenosylmethionine in mycobacteria. Similar effect was described in the case of PAS, which through inhibition of tetrahydrofolate production affects one-carbon metabolism [32].

Table 3
The MIC (μg/mL) of PAS, **10c** and its sodium salt **10cNa** against *M. tuberculosis* H37Ra overproducing FolP1, FolC, DfrA or RibD proteins.

	pVV2[a]	pVV2-*folP1*	pVV2-*folC*	pVV2-*dfrA*	pVV2-*ribD*
PAS	0.02	0.02	0.02	>5	2.5
10c	8	8	8	8	8
10cNa	8	8	8	8	8

[a] *Mtb* H37Ra with the empty vector.

2.3.3.3. Complementation of antimycobacterial activity of 10c by methionine. It was demonstrated that antimycobacterial activity of PAS can be antagonized by supplementation with exogenous methionine. To find out whether exogenous methionine can antagonize also antimycobacterial activity of **10c**, the effect of this compound to the growth of *Mtb* H37Ra cells was analyzed in the presence of 0, 50, 100 and 250 μM methionine in culture media. We observed that the presence of 50 μM methionine could reverse the inhibitory activity of compound **10c** up to 1x its MIC (Fig. 4). In the case of PAS 50 μM methionine reversed the inhibitory activity up to 40x its MIC. These data suggest that **10c** affects the metabolism of methionine by inhibition of an unknown molecular target.

2.3.4. In silico exploration of binding of compound 10c to mycobacterial methionyl-tRNA synthetase (mtMetRS)

Compound **10d** was previously reported as a candidate inhibitor of *E. coli* methionyl-tRNA synthetase [15]. The most significant compound of the current study, compound **10c** is a close structural derivative, having an extra hydroxyl on the benzene ring (thus being a derivative of 4-aminosalicylic acid rather than 4-aminobenzoic acid). Therefore, we decided to perform an *in silico* simulation to elucidate whether compound **10c** could bind to mycobacterial methionyl-tRNA synthetase (mtMetRS). The binding could partially constitute the mechanism of the antimycobacterial activity of the compound or, at least, provide hints for the future development of the fragment towards more efficient inhibitors of the enzyme.

The inspection of the complex of mtMetRS with catalytic intermediate methionyl-adenylate (pdb id: 6ax8) revealed missing coordinates of sidechain atoms of several residues in the loop Asn295–Val308. This

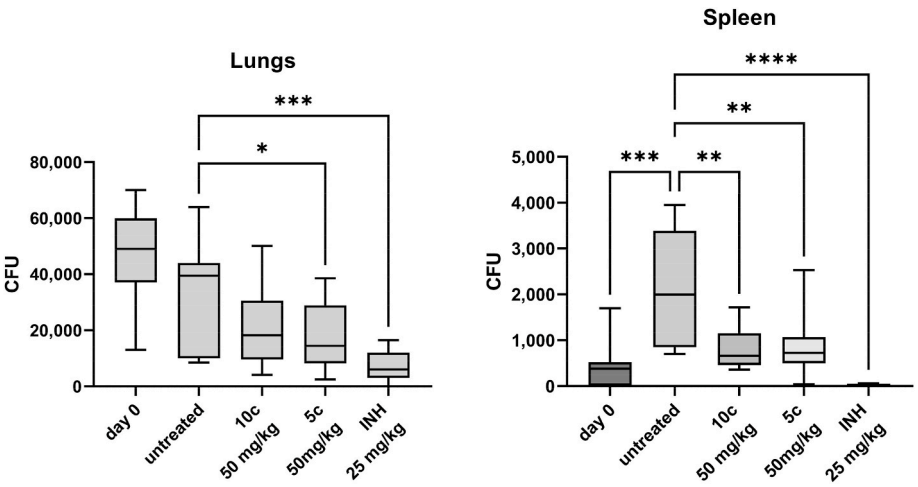

Fig. 2. Antimycobacterial efficacy *in vivo* of compounds **10c** (as a sodium salt) and **5c** (sodium salt dihydrate) in comparison with isoniazid (INH). The boxes cover the 25th to 75th percentile, horizontal line in the box is median, and the whiskers represent minimal/maximal values. (* - $P \leq 0.05$; ** - $P \leq 0.01$; *** - $P \leq 0.001$; **** - $P \leq 0.0001$).

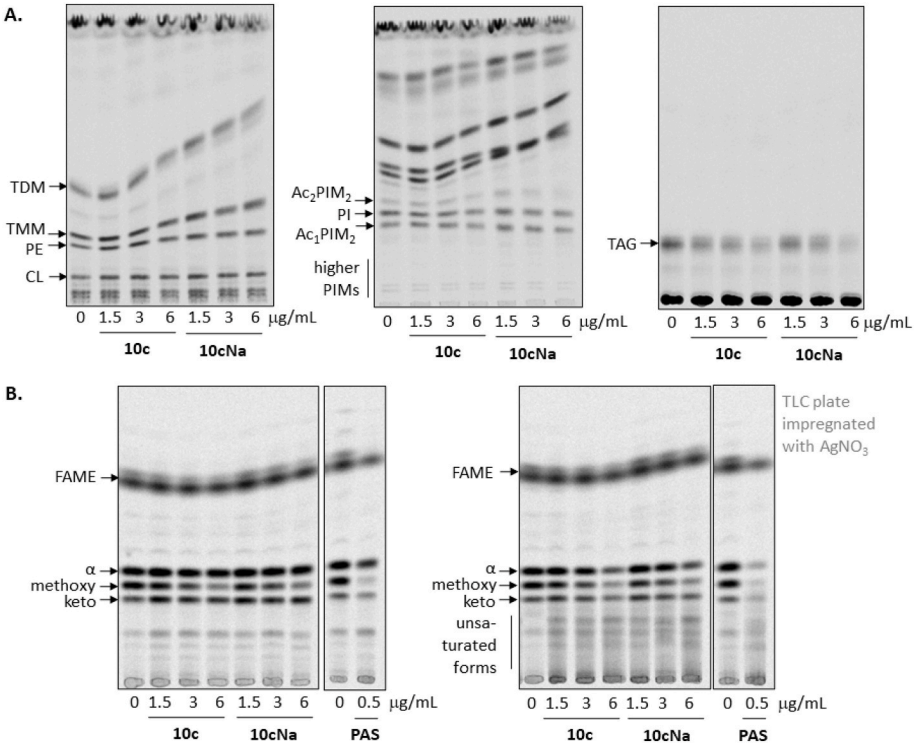

Fig. 3. The effect of **10c** and its sodium salt **10cNa** on lipids (A) and fatty acids (B) of *Mtb* H37Rv. (A) The lipids were extracted from the cells *Mtb* H37Rv cultivated in the presence of different concentrations of **10c/10cNa** and metabolically labeled with ^{14}C acetate. Isolated lipids were separated in Solvent I (left), Solvent II (in the middle), or Solvent III (right), and visualized by autoradiography. (B) Fatty acids were extracted from the cells *Mtb* H37Rv cultivated as described above, derivatized to corresponding methyl esters, loaded on the standard (left) or $AgNO_3$ impregnated (right) TLC plate, separated in Solvent IV and visualized by autoradiography. TMM – trehalose monomycolates, TDM – trehalose dimycolates, PE - phosphatidylethanolamine, CL - cardiolipin, PI - phosphatidylinositol, PIM – phosphatidylinositol mannosides, TAG - triacylglycerols, FAME – fatty acid methyl esters; α-, methoxy-, keto-, unsaturated forms - refer to the different forms of mycolic acids methyl esters.

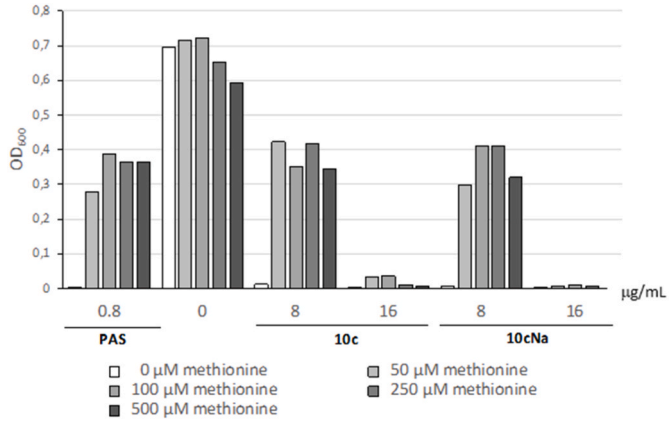

Fig. 4. Antimycobacterial activity of 10c/10cNa in the presence of different concentrations of methionine in culture media. The cells of *M. tuberculosis* H37Ra were treated with PAS or different concentrations of 10c/10cNa and grown in the presence of 0, 50, 100, 250 or 500 µM methionine in media. The growth was monitored after 15 days by measuring the optical density of the cultures at 600 nm.

loop is in close contact with the adenine core of the substrate/intermediate and is therefore important for binding. The flexibility of this loop and the inherited uncertainty in positions of residues important for binding led us to utilize the induced fit docking protocol – assigning flexibility to pocket sidechains in the energy refinement post-docking optimization.

The docked pose of **10c** in mtMetRS was then used as an input for subsequent molecular dynamics (MD) simulations (three production runs of 80 ns) to refine the ligand-receptor complex. The MD simulations proved that the initial docking pose (Fig. 5A, magenta carbons) was not stable and within the first 15–20 ns of the production phase runs, a new pose was discovered (green carbons). During this transition, the position of the quinoline core of the ligand remained similar, but there was a significant shift in the position of the 4-aminosalicylic acid core. This shift was accompanied by a movement of the flexible loop Asn295–Val308 towards the ligand, resulting in additional stabilization by a newly formed strong ionic interaction between Lys299 side chain and the carboxylate of the ligand (Fig. 5A). The MD-optimised pose (Fig. 5B) then remained stable in all three production runs, although the interaction to Lys299 broke occasionally. The pose (Fig. 5, panels B and C) is stabilized by up to three H-bonds and one ionic interaction (to Lys299). The occupancies of the interactions of individual production runs are stated in Table 4. The quinoline core occupies the lipophilic area of the binding pocket formed by residues Ala9, Ile10, Ala11, Trp228, Ala231, Leu232 and Ile264. The MD-optimised pose can be rationalized by comparison with the binding mode of the crystallographic methionyl-adenylate (Met-Ade) intermediate (Fig. 5D). The quinoline core of compound **10c** occupies the same hydrophobic space as the hydrophobic sidechain of the methionine (feature A). The α-amino moiety of methionine, respectively the NH of the amidic linker of **10c** interact with Ile10 (feature B). The position of the carbonyl oxygen of **10c** corresponds to its carbonyl counterpart in the Met-Ade (feature C). The phenolic hydroxyl of **10c** takes the role of the Met-Ade phosphate oxygen in the common interaction with Tyr12 (feature D). Both **10c** and Met-Ade form H-bond to His21 (feature E). Additional outputs from the trajectory analyses (RMSD for protein and ligand) can be found in Supplementary Data (Fig. S3 and Fig. S4).

The MD simulations confirmed the possibility of **10c** binding to the active site of mtMetRS and exemplified the importance of stabilization of the flexible adenine binding loop in ligand-receptor interactions. The flexibility of this loop is the reason why compound **10c** could effectively stabilize the protein, despite being significantly smaller in size in comparison to Met-Ade (missing the spatial equivalent to the adenine core, Fig. 5D). Similar simulations could give background for the structure-optimization of similar ligands to enhance the stabilization of the adenine binding loop.

2.3.5. In vitro metabolism in human liver microsomes

2.3.5.1. In vitro human liver microsomal stability testing. The ammonium

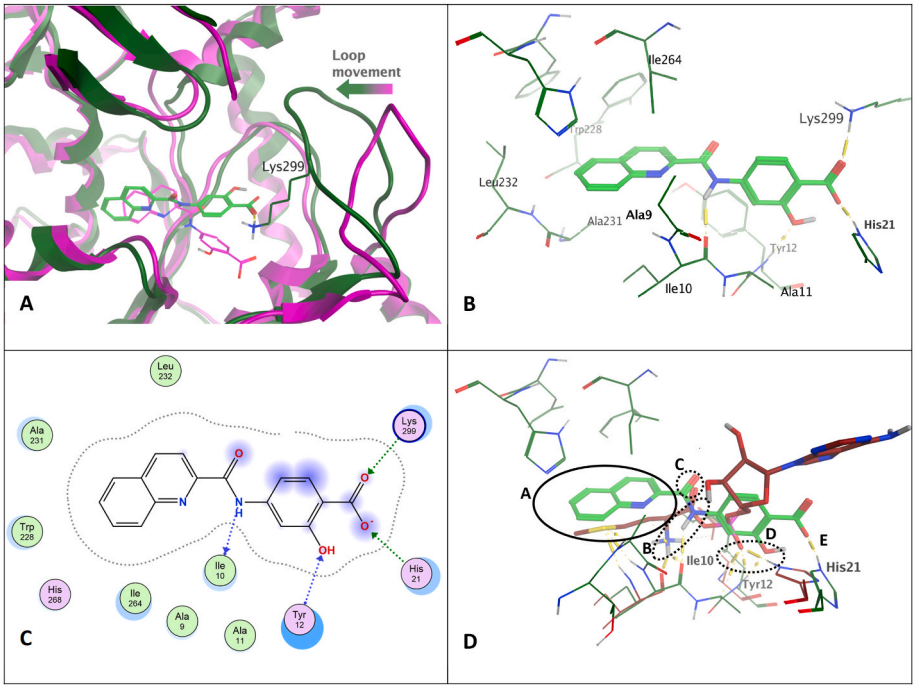

Fig. 5. *In silico* binding of **10c** to mtMetRS. **A** – Comparison of the initial pose after docking (magenta) to the final MD-optimised pose (green); **B** – MD-modified pose in 3D; **C** – MD-modified pose as a 2D ligand-protein interaction diagram; **D** – Comparison to the binding mode of the natural Met-adenylate intermediate (brown, pdb: 6ax8), the common features of the binding mode are highlighted by ellipses.

Table 4
Abundance of selected ligand-receptor interactions in the production runs of MD simulation of **10c**-mtMetRS complex.

Donor	Acceptor	Interaction	Occupancy[a]		
			repl_1	repl_2	repl_3
His21-sc	Ligand COO^-	H-bond	70%	47%	62%
Tyr12-bb	Ligand OH	H-bond	76%	68%	58%
Lys299-sc	Ligand COO^-	H-bond/ionic	11%	47%	38%
Ligand CONH	Ile10-bb	H-bond	10%	36%	36%

[a] Calculated for the last 60 ns of 80 ns production runs. bb - interaction to backbone; sc - interaction to sidechain.

salt of compound **10c** (used for better solubility of the compound) and its lactone form **10c'** (both 3 μM) were incubated with Human Liver Microsomes (HLM) at physiological pH at 5 different time points over the course of 45 min experiment to determine the *in vitro* human microsomal stability [33]. The incubation reactions were stopped after a given time point (0, 5, 15, 30, 45 min) and then the samples were analyzed by HPLC-MS system using the chromatographic conditions mentioned in Supplementary Data (Section 8). The value of $t_{1/2}$, the value of k and the intrinsic clearance (CL_{int}) for the ammonium salt of compound **10c** and its lactone form were calculated from the HPLC-MS records (see Table S6). The obtained values were compared with known fast and slow metabolically degraded standards of verapamil and diazepam (see Table S7 in Supplementary Data). The following values were calculated for the ammonium salt of compound **10c**, $t_{½}$ = 630 min (k = 0.0011) and CL_{int} = 2.2 μl/min/mg of protein and for its lactone form **10c'**, $t_{½}$ = 11 min (k = 0.0611) and CL_{int} = 122.3 μl/min/mg of protein. It can be concluded that compound **10c** has a relatively high value of $t_{½}$ and low CL_{int}, implying that the molecule is very metabolically stable, while its lactone showed absolutely opposite metabolic behavior and is quickly biotransformed to its active open form. When compared to PAS that has a short half-life of 48 min [9], our compound **10c** overcame PAS main drawback and hence lower doses of the compound are needed.

2.3.5.2. Identification of metabolites. For experimental determination of phase I metabolites formed *in vitro*, the ammonium salt of compound **10c** and its lactone **10c'** (both 90 μM) were incubated with HLM for 3 h under given conditions [34]. See Supplementary Data. After incubation of compound **10c** salt with HLM, two main metabolites were detected in positive ion mode, M1 (m/z = 175.0500) and M2 (m/z = 154.0498). The potential structures (Fig. 6) of the main metabolites were designed on the basis of high-resolution mass spectrometry measurement, empirical formulae predicted by software, isotopic representation of individual elements, and their chromatographic behavior. These metabolites appear to be formed as a result of metabolic cleavage of the amide bond.

In the case of lactone **10c'**, three major metabolites were detected. The main path of biotransformation is the opening of the lactone form to the free acid M3 (m/z = 310.0822). Furthermore, the metabolites M1 and M2 mentioned above were formed from the lactone as well. The suggested structures of the M1-M3 metabolites are shown in Fig. 6.

Interestingly, there was no oxidation or hydroxylation after HLM incubation. The recorded metabolic change could also lead to a potentiation of the antimycobacterial effect of compound **10c** and its lactone, as the detected metabolite M2 (PAS) also showed antitubercular activity.

3. Experimental

3.1. General

All reagents and solvents (unless stated otherwise) were purchased from Sigma-Aldrich (Schnelldorf, Germany) and used without further purification. Reaction progress and purity of products were monitored using Silica 60 F_{254} TLC plates (Merck, Darmstadt, Germany). Flash chromatography of the final compounds was performed on a puriFlash XS420+ (Interchim, Montluçon, France) with original columns (spherical silica, 30 μm) provided by the same company. The mobile phase was ethyl acetate (EtOAc) in hexane (Hex), gradient elution 0–100%, and detection was performed by UV-VIS detector at 254 nm and 280 nm. The NMR spectra were recorded on a Varian VNMR S500 (Varian, Palo Alto,

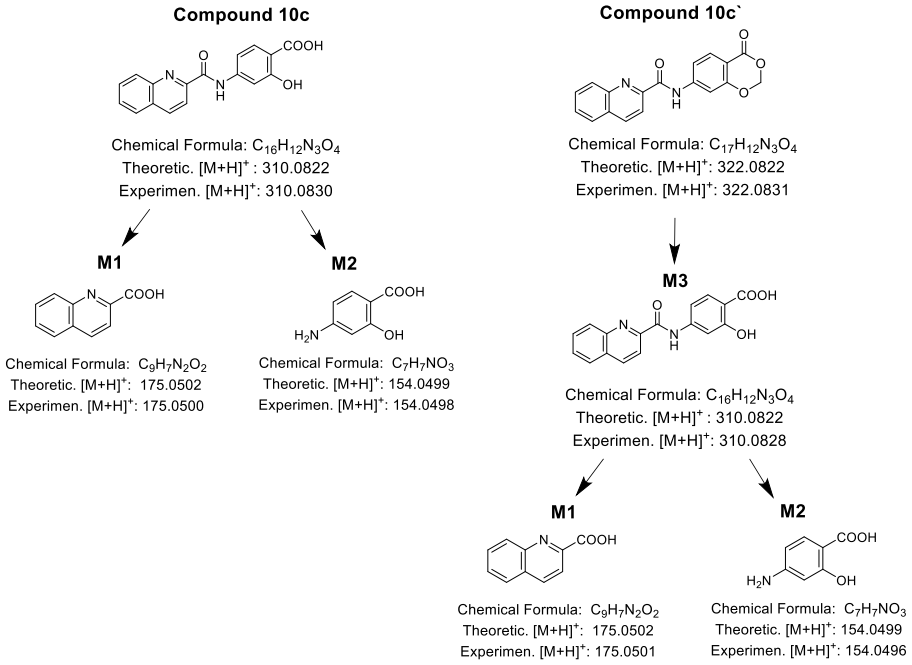

Fig. 6. Schematic illustration of the suggested structures of metabolites for compound **10c** and its lactone **10c**′ after incubation with human liver microsomes (HLM).

CA, USA) at 500 MHz for ^{1}H and 126 MHz for ^{13}C. The spectra of compounds **6c**, **7c**, **9c**, **10c′, 2d, 6d and 4-methoxypicolinamide** were measured on Jeol JNM-ECZ600R at 600 MHz for ^{1}H and 151 MHz for ^{13}C. The spectra were recorded in DMSO-d_6 at ambient temperature. The chemical shifts reported as δ values in ppm are indirectly referenced to tetramethylsilane (TMS) via the solvent signal (2.49 for ^{1}H and 39.7 for ^{13}C in DMSO-d_6). IR spectra were recorded on a NICOLET 6700 FT-IR spectrophotometer (Nicolet, Madison, WI, USA) using the ATR-Ge method. Elemental analysis was done on a Vario MICRO cube Element Analyzer (Elementar Analysensysteme, Hanau, Germany) with values given as a percentage. Compounds **10c** and **10c'** were analyzed by an UHLPC Dionex Ultimate 3000 RS (Thermo Fisher Scientific, Bremen, Germany) to obtain HPLC-UV purity. The samples were analyzed by the HPLC method described in Supplementary Data, section 8. Gradient LC analysis with UV detection (254 nm) confirmed $\geq$95% purity. Yields are given in percentage and refer to the amount of pure product after all purification steps. Log*P* values were calculated using ChemDraw v20.0. (PerkinElmer Informatics, Waltham, MA, USA).

3.2. Chemistry

Final compounds were obtained by amidation. Two different amide formation reactions were utilized.

3.2.1. General procedure 1 – amidation via acyl imidazoles

Series **a**, **c** and **d** were prepared by this method. In a 10 mL test tube, 2 mmol of selected pyridine carboxylic acid was added to 2.2 mmol of CDI and mixed thoroughly by shaking, then heated for 1 min with an air dryer. Then 2 mL of anhydrous DMSO (series **c** and **d**) or 10 mL of anhydrous DCM (series **a**) were added to the mixture and bubbling occurred immediately. The mixture was left to stir for 30 min at room temperature to achieve full activation. In a separate 10 mL test tube, 2 mmol of corresponding amine were dissolved in 1 mL of anhydrous DMSO or DCM. In the final step, the dissolved amine was added to the contents of the first vial and left to react overnight at room temperature. On the following day, for compounds in DMSO, the mixture was acidified dropwise with 5% HCl until a solid precipitate was formed. The crystals were filtered and re-crystallized from water and ethanol (30 mL water and 5 mL ethanol). For reactions in DCM, the reaction mixture was washed with water (2x 15 mL) and brine (10 mL). The organic layer was then stirred with anhydrous Na_2SO_4 for 5 min and then Na_2SO_4 was filtered off using cotton. The filtrate was evaporated under reduced pressure and adsorbed on silica gel to purify it with column flash chromatography using gradient elution 0–100% EtOAc in hexane.

3.2.2. General procedure 2 – amidation via acyl chlorides

Series **b** was prepared by this method. 2 mmol of selected pyridine carboxylic acid was dissolved in 15 mL of anhydrous DCM in a 50 mL Erlenmeyer flask with stirring. Another 10 mL Erlenmayer flask was charged with 3 mL of anhydrous DCM and 2 mmol of oxalyl chloride. The mixture was mixed and added dropwise to the contents of the first flask. Two drops of DMF were then added and stirred mixture was left covered with parafilm and stirred at room temperature for 30 min to afford activation. In another Erlenmayer flask, 2 mmol of the corresponding amine was added to 20 mL of anhydrous DCM and stirred. Pyridine (3 mmol) was then added to the amine solution, and the mixture was covered with parafilm and put into an ice bath. After 30 min, the content of the first Erlenmeyer flask (acyl chloride) was added dropwise to the amine mixture while stirring in the ice bath for 15 min and the reaction was left to stir at room temperature overnight. The organic layer was extracted with water (2x 15 mL) and brine (10 mL). The organic layer was then stirred with anhydrous Na_2SO_4 for 5 min and then Na_2SO_4 was filtered off using cotton. The obtained solution was evaporated under reduced pressure and adsorbed on silica gel to purify it with column flash chromatography using gradient elution 0–100% EtOAc in hexane.

3.2.3. Synthesis of non-substituted carboxamides

(Picolinamide, 4-methoxypicolinamide, and quinoline-2-carboxamide). In a 25 mL test tube, 2 mmol of selected pyridine carboxylic acid was added to 2.2 mmol of CDI and mixed thoroughly by shaking then heated for 1 min with an air dryer. Then 5 mL of anhydrous DCM was added to the mixture and bubbling occurred immediately. The mixture was left to stir for 30 min at room temperature to achieve full activation. After that time an excess of concentrated aqueous ammonia (35% w/w) was added and the mixture was left to stir overnight. On the following day, the mixture was evaporated under reduced pressure and the solid was washed with cold water.

3.3. Analytical data

3.3.1. N-(pyrazin-2-yl)isonicotinamide (1a)

White solid; Yield 12%; ^{1}H NMR (500 MHz, DMSO-d_6) δ 11.43 (s, 1H), 9.42 (d, J = 1.5 Hz, 1H), 8.80–8.76 (m, 3H), 8.50 (dd, J = 2.6, 1.5 Hz, 1H), 8.45 (d, J = 2.6 Hz, 1H), 7.94–7.91 (m, 3H); ^{13}C NMR (126 MHz, DMSO-d_6) δ 165.1, 150.5, 148.8, 142.9, 140.8, 140.7, 139.0, 137.7, 122.1; IR (ATR-Ge, cm^{-1}): 3103 (NH amidic stretch), 1697 (amidic CO stretch), 1592, 1536, 1506 (C–C aromatic stretch); Elemental analysis: calculated for $C_{10}H_8N_4O$ (MW 200.20) 59.99% C; 4.03% H; 27.99% N; found 59.82% C; 4.00% H; 28.20% N; CAS Registry Number 93906-19-5.

3.3.2. N-(pyrazin-2-yl)picolinamide (2a)

Light beige solid; Yield 35%; M. p. 215–217 °C; ^{1}H NMR (500 MHz, DMSO-d_6) δ 10.58 (s, 1H), 9.49 (d, J = 1.6 Hz, 1H), 8.78–8.73 (m, 1H), 8.50–8.44 (m, 2H), 8.24–8.19 (m, 1H), 8.15–8.08 (m, 1H), 7.77–7.70 (m, 1H); ^{13}C NMR (126 MHz, DMSO-d_6) δ 162.5, 148.9, 148.3, 147.7, 143.2, 140.2, 138.7, 136.4, 127.9, 122.7; IR (ATR-Ge, cm^{-1}): 3150 (NH amidic stretch), 1695 (amidic CO stretch), 1531, 1517, 1489 (C–C aromatic stretch); Elemental analysis: calculated for $C_{10}H_8N_4O$ (MW 200.20) 59.99% C; 4.03% H; 27.99% N; found 59.69% C; 3.84% H; 27.99% N; CAS Registry Number 94782-82-8.

3.3.3. 4-Methoxy-N-(pyrazin-2-yl)picolinamide (3a)

White solid; Yield 18%; M. p. 241–242 °C; ^{1}H NMR (500 MHz, DMSO-d_6) δ 10.57 (s, 1H), 9.48 (d, J = 1.5 Hz, 1H), 8.56 (d, J = 5.7 Hz, 1H), 8.50–8.43 (m, 2H), 7.70 (d, J = 2.6 Hz, 1H), 7.28 (dd, J = 5.7, 2.6 Hz, 1H), 3.95 (s, 3H). ^{13}C NMR (126 MHz, DMSO-d_6) δ 167.1, 162.3, 150.4, 150.2, 147.6, 143.2, 140.8, 136.3, 113.7, 108.6, 56.1; IR (ATR-Ge, cm^{-1}): 3200 (NH amidic stretch), 1701 (amidic CO stretch), 1630, 1610, 1587 (C–C aromatic stretch); Elemental analysis: calculated for $C_{11}H_{10}N_4O_2$ (MW 230.23) 57.39% C; 4.38% H; 24.34% N; found 57.00% C; 4.20% H; 24.15% N; CAS Registry Number 1795294-30-2.

3.3.4. 2-Methyl-N-(pyrazin-2-yl)isonicotinamide (4a)

Beige solid; Yield 59%; M. p. 234–235 °C; ^{1}H NMR (500 MHz, DMSO-d_6) δ 11.77 (s, 1H), 9.40 (s, 1H), 8.93–8.87 (m, 1H), 8.56–8.51 (m, 1H), 8.49 (t, J = 2.2 Hz, 1H), 8.31 (s, 1H), 8.22–8.17 (m, 1H), 2.80 (s, 3H). ^{13}C NMR (126 MHz, DMSO-d_6) δ 164.7, 161.5, 149.7, 149.0, 144.8, 139.5, 137.4, 136.1, 118.4, 118.3, 23.5. IR (ATR-Ge, cm^{-1}): 3090 (NH amidic stretch), 1688 (amidic CO stretch), 1641, 1608, 1550 (C–C aromatic stretch); Elemental Analysis: calculated for $C_{11}H_{10}N_4O$ (MW 214.23) 61.67% C; 4.71% H; N, 26.15%; found 61.43% C; 4.53% H; 25.98% N.

3.3.5. 6-Chloro-N-(pyrazin-2-yl)nicotinamide (5a)

White solid; Yield 24%; ^{1}H NMR (500 MHz, DMSO-d_6) δ 11.45 (s, 1H), 7.86 (d, J = 3.0 Hz, 2H), 7.65 (d, J = 2.5 Hz, 2H), 6.36 (s, 2H). ^{13}C NMR (126 MHz, DMSO-d_6) δ 164.7, 154.3, 150.4, 149.2, 140.3, 139.4, 137.3, 136.2, 125.7, 128.5. IR (ATR-Ge, cm^{-1}): 3120 (NH amidic stretch), 1699 (amidic CO stretch), 1625, 1578, 1566 (C–C aromatic stretch); Elemental Analysis: calculated for $C_{10}H_7ClN_4O$ (MW 234.64) 51.19% C; 3.01% H; 23.88% N; found 51.23% C; 3.03% H; 23.88% N; CAS Registry Number 352228-91-2.

3.3.6. 6-Chloro-N-(pyrazin-2-yl)picolinamide (6a)

White solid; Yield 28%; ^{1}H NMR (500 MHz, DMSO-d_6) δ 10.41 (s, 1H), 9.44 (d, J = 1.5 Hz, 1H), 8.51–8.43 (m, 2H), 8.21–8.11 (m, 2H), 7.89–7.81 (m, 1H); ^{13}C NMR (126 MHz, DMSO-d_6) δ 161.5, 149.5, 149.3, 147.6, 143.2, 142.1, 140.9, 136.6, 128.5, 122.1; IR (ATR-Ge, cm^{-1}): 3090 (NH amidic stretch), 1703 (amidic CO stretch), 1579, 1532, 1516 (C–C aromatic stretch); Elemental analysis: calculated for $C_{10}H_7ClN_4O$ (MW 234.64): 51.19% C; 3.01% H; 23.88% N; found 50.90% C; 2.85% H; 23.84% N; CAS Registry Number 94782-82-8.

3.3.7. N-(pyrazin-2-yl)-5-(trifluoromethyl)picolinamide (7a)

Beige solid; Yield 54%; ^{1}H NMR (500 MHz, $CDCl_3$) δ 10.41 (s, 1H), 9.76 (d, J = 1.5 Hz, 1H), 8.96–8.92 (m, 1H), 8.47 (d, J = 8.0 Hz, 1H), 8.43 (d, J = 2.5 Hz, 1H), 8.36 (dd, J = 2.5, 1.5 Hz, 1H), 8.21 (dd, J = 8.0, 2.5 Hz, 1H); ^{13}C NMR (126 MHz, $CDCl_3$) δ 161.1, 151.6, 147.6, 145.5 (q, J = 4.0 Hz), 142.5, 140.8, 137.0, 135.3 (q, J = 3.6 Hz), 129.7 (q, J = 33.5 Hz), 122.9 (q, J = 273.0 Hz); IR (ATR-Ge, cm^{-1}): 3200 (NH amidic stretch), 1701 (amidic CO stretch), 1630, 1610, 1587 (C–C aromatic stretch); Elemental analysis: calculated for $C_{11}H_7F_3N_4O$ (MW 268.20): 49.26% C; 2.63% H; 20.89% N.

3.3.8. 2-Chloro-6-methyl-N-(pyrazin-2-yl)isonicotinamide (9a)

White solid; Yield 38%; ^{1}H NMR (500 MHz, DMSO-d_6) δ 11.42 (s, 1H), 9.38 (d, J = 1.5 Hz, 1H), 8.50 (dd, J = 2.5, 1.5 Hz, 1H), 8.46 (d, J = 2.5 Hz, 1H), 7.84 (s, 1H), 7.80 (s, 1H), 2.54 (s, 3H); ^{13}C NMR (126 MHz, DMSO-d_6) δ 163.8, 160.3, 149.9, 148.6, 144.5, 142.9, 140.8, 137.5, 121.0, 119.8, 23.8; IR (ATR-Ge, cm^{-1}): 3042 (NH amidic stretch), 1682 (amidic CO stretch), 1594, 1545, 1463 (C–C aromatic stretch); Elemental analysis: calculated for $C_{11}H_9ClN_4O$ (MW 248.67) 53.13% C; 3.65% H; 22.53% N; found 53.10% C; 3.53% H; 22.21% N; CAS Registry Number 1915230-95-3.

3.3.9. N-(pyrazin-2-yl)quinoline-2-carboxamide (10a)

White solid; Yield 32%; ^{1}H NMR (500 MHz, DMSO-d_6) δ 10.79 (s, 1H), 9.55 (d, J = 1.5 Hz, 1H), 8.68 (d, J = 8.6 Hz, 1H), 8.55–8.46 (m, 2H), 8.29 (d, J = 8.6 Hz, 1H), 8.26 (d, J = 8.6 Hz, 1H), 8.13 (dd, J = 8.2, 1.4 Hz, 1H), 7.92 (ddd, J = 8.2, 6.8, 1.4 Hz, 1H), 7.78 (ddd, J = 8.2, 6.8, 1.4 Hz, 1H); ^{13}C NMR (126 MHz, DMSO-d_6) δ 162.7, 148.4, 147.7, 145.9, 143.2, 140.8, 138.9, 136.3, 131.2, 129.6, 129.4, 129.0, 128.3, 118.7; IR (ATR-Ge, cm^{-1}): 3057 (NH amidic stretch), 1701 (amidic CO stretch), 1567, 1526, 1504 (C–C aromatic stretch); Elemental analysis: calculated for $C_{14}H_{10}N_4O$ (MW 250.26): 67.19% C; 4.03% H; 22.39% N; found 66.92% C; 3.85% H; 22.06% N; CAS Registry Number 2327399-08-4.

3.3.10. N-(6-chloropyrazin-2-yl)nicotinamide (1b)

White solid; Yield 39%; ^{1}H NMR (500 MHz, DMSO-d_6) δ 11.70 (s, 1H), 9.41 (s, 1H), 8.81–8.76 (m, 2H), 8.57 (s, 1H), 7.95–7.90 (m, 2H); ^{13}C NMR (126 MHz, DMSO-d_6) δ 165.1, 150.4, 148.2, 145.7, 140.3, 139.3, 135.3, 122.1; IR (ATR-Ge, cm^{-1}): 3064 (NH amidic stretch), 1687 (CO amidic stretch), 1542, 1501 (C–C aromatic stretch). Elemental Analysis: calculated for $C_{10}H_7ClN_4O$ (MW 234.64) 51.19% C; 3.01% H; 23.88% N; found 50.80% C; 2.97% H; 23.61% N; CAS Registry Number 1564769-51-2.

3.3.11. N-(6-chloropyrazin-2-yl)isonicotinamide (2b)

White solid; Yield 17%; ^{1}H NMR (500 MHz, DMSO-d_6) δ 10.78 (s, 1H), 9.42 (s, 1H), 8.75 (d, J = 4.7 Hz, 1H), 8.57 (s, 1H), 8.20 (d, J = 7.7 Hz, 1H), 8.11 (td, J = 7.7, 1.7 Hz, 1H), 7.74 (dd, J = 7.7, 4.7 Hz, 1H); ^{13}C NMR (126 MHz, DMSO-d_6) δ 162.8, 149.0, 148., 147.1, 145.9, 139.3, 138.7, 134.4, 128.1, 122.9. IR (ATR-Ge, cm^{-1}): 3065 (NH amidic stretch), 1698 (amidic CO stretch), 1563, 1527, 1516 (C–C aromatic stretch); Elemental analysis: calculated for $C_{10}H_7ClN_4O$ (MW 234.64) 51.19% C; H, 3.01% H; N, 23.88% N; found: 50.87% C; 2.84% N; 23.49% N; CAS Registry Number 1564925-55-8.

3.3.12. N-(6-chloropyrazin-2-yl)-4-methoxypicolinamide (3b)

Beige solid; Yield 22%; ^{1}H NMR (500 MHz, DMSO-d_6) δ 10.78 (s, 1H), 9.42 (s, 1H), 8.61–8.55 (m, 2H), 7.70 (d, J = 2.5 Hz, 1H), 7.32–7.27 (m, 1H), 3.95 (s, 3H). ^{13}C NMR (126 MHz, DMSO-d_6) δ 167.4, 162.9, 150.7, 147.3, 146.2, 139.7, 134.7, 114.1, 109.1, 56.4. IR (ATR-Ge, cm^{-1}): 3210 (NH amidic stretch), 1710 (amidic CO stretch), 1640, 1610, 1567 (C–C aromatic stretch); Elemental analysis: calculated for $C_{11}H_9ClN_4O_2$ (MW 264.67) 49.92% C; 3.43% H; 21.17% N; found: 49.82% C; 3.20% H; 20.97% N.

3.3.13. ***N-(6-chloropyrazin-2-yl)-2-methylisonicotinamide (4b)***

White solid; Yield 20%; ^{1}H NMR (500 MHz, DMSO-d_6) δ 12.05 (s, 1H), 9.39 (s, 1H), 8.90 (d, J = 5.9 Hz, 1H), 8.62 (s, 1H), 8.31 (s, 1H), 8.19 (dd, J = 5.9, 1.8 Hz, 1H), 2.80 (s, 3H); ^{13}C NMR (126 MHz, DMSO-d_6) δ 163.5, 155.7, 147.8, 146.4, 145.8, 143.4, 139.8, 135.3, 125.8, 122.4, 20.4; IR (ATR-Ge, cm^{-1}): 3178 (NH amidic stretch), 1699 (amidic CO stretch), 1622, 1603, 1588 (C–C aromatic stretch); Elemental analysis: calculated for $C_{11}H_9ClN_4O$ (MW 248.67) 53.13% C; 3.65% H; 22.53% N; found: 52.86% C; 3.47% H; 22.15% N; CAS Registry Number 1976925-03-7.

3.3.14. ***6-Chloro-N-(6-chloropyrazin-2-yl)nicotinamide (5b)***

White solid; Yield 44%; ^{1}H NMR (500 MHz, DMSO-d_6) δ 11.72 (s, 1H), 9.40 (s, 1H), 8.99 (d, J = 1.8 Hz, 1H), 8.56 (s, 1H), 8.40 (dd, J = 8.3, 2.5 Hz, 1H), 7.70 (d, J = 8.3 Hz, 1H); ^{13}C NMR (126 MHz, DMSO-d_6) δ 164.1, 153.7, 150.1, 148.2, 145.6, 139.8, 139.2, 135.2, 128.6, 124.3; IR (ATR-Ge, cm^{-1}): 3099 (NH amidic stretch), 1678 (amidic CO stretch), 1578, 1554, 1545 (C–C aromatic stretch); Elemental analysis: calculated for $C_{10}H_6Cl_2N_4O$ (MW 269.09): 44.64% C; 2.25% H; 20.82% N; found 44.26% C; 2.20% H; 20.45% N.

3.3.15. ***N-(6-chloropyrazin-2-yl)-5-(trifluoromethyl)pyrazine-2-carboxamide (7b)***

Beige solid; Yield 38%; ^{1}H NMR (500 MHz, DMSO-d_6) δ 11.00 (s, 1H), 9.40 (s, 1H), 9.18–9.14 (m, 1H), 9.08 (s, 1H), 8.61 (s, 1H), 8.53 (dd, J = 8.1, 2.3 Hz, 1H), 8.36 (d, J = 8.1 Hz, 1H); ^{13}C NMR (126 MHz, DMSO-d_6) δ 162.1, 151.9, 147.1, 145.9 (d, J = 4.0 Hz) 139.7, 136.3 (q, J = 3.6 Hz), 134.8, 128.3 (q, J = 32.5 Hz), 123.4 (q, J = 273.0 Hz), 123.3; IR (ATR-Ge, cm^{-1}): 3298 (NH amidic stretch), 1712 (amidic CO stretch), 1640, 1621, 1598 (C–C aromatic stretch); Elemental analysis: calculated for $C_{10}H_5ClF_3N_5O$ (MW 303.63): 39.56% C; 1.66% H; 23.07% N; CAS Registry Number 1772118-52-1.

3.3.16. ***N-(6-chloropyrazin-2-yl)quinoline-2-carboxamide (10b)***

White solid; Yield 55%; ^{1}H NMR (500 MHz, DMSO-d_6) δ 11.02 (s, 1H), 9.50 (s, 1H), 8.68 (d, J = 8.4 Hz, 1H), 8.60 (s, 1H), 8.28 (t, J = 8.2 Hz, 2H), 8.14 (d, J = 7.3 Hz, 1H), 7.93 (dd, J = 8.4, 6.8 Hz, 1H), 7.79 (dd, J = 8.2, 6.8 Hz, 1H); ^{13}C NMR (126 MHz, DMSO-d_6) δ 163.0, 148.2, 147.2, 146.0, 145.9, 139.4, 138.9, 134.4, 131.2, 129.7, 129.5, 129.1, 128.3, 118.7; IR (ATR-Ge, cm^{-1}): 3311 (NH amidic stretch), 1705 (amidic CO stretch), 1564, 1530, 1505 (C–C aromatic stretch). Elemental analysis: calculated for $C_{14}H_9ClN_4O$ (MW 284.70) 59.06% C; 3.19% H; 19.68% N; found: 59.00% C; 3.01% H; 19.35% N. CAS Registry Number 1917408-22-0.

3.3.17. ***2-Hydroxy-4-(isonicotinamido)benzoic acid (1c)***

White solid; Yield 47%; ^{1}H NMR (500 MHz, DMSO-d_6) δ 10.63 (s, 1H), 8.82–8.74 (m, 2H), 7.87–7.83 (m, 2H), 7.76 (d, J = 8.6 Hz, 1H), 7.55 (s, 1H), 7.45 (d, J = 2.0 Hz, 1H), 7.27 (dd, J = 8.6, 2.0 Hz, 1H); ^{13}C NMR (126 MHz, DMSO-d_6) δ 171.9, 164.70, 162.3,150.5, 144.3, 141.9, 134.7, 131.0, 121.8, 120.0, 110.9, 110.6, 107.4, 98.7; IR (ATR-Ge, cm^{-1}): 3313 (phenolic O–H stretch), 3077 (amidic *N*–H stretch), 2843 (carboxylic O–H stretch), 1674 (carbonyl C═O stretch), 1620, 1599, 1562 (aromatic C–C stretch), 1235 (carboxylic C–O stretch), 910 (carboxylic O–H bend); Elemental analysis: calculated for $C_{13}H_{10}N_2O_4$ (MW 258.23) 60.47% C; 3.90% H; 10.85% N; found: 60.55% C; 3.78% H; 10.77% N. CAS Registry Number 32476-99-6.

3.3.18. ***2-Hydroxy-4-(picolinamido)benzoic acid (2c)***

White solid; Yield 20%;^{1}H NMR (500 MHz, DMSO-d_6) δ 11.36 (s, 1H), 10.85 (s, 1H), 8.80–8.72 (m, 1H), 8.17 (d, J = 7.7 Hz, 1H), 8.08 (td, J = 7.7, 1.8 Hz, 1H), 7.76 (d, J = 8.7 Hz, 1H), 7.74–7.65 (m, 2H), 7.49 (dd, J = 8.7, 1.8 Hz, 1H); ^{13}C NMR (126 MHz, DMSO-d_6) δ 171.8, 163.3, 162.1, 149.7, 148.7, 144.9, 138.4, 131.1, 127.4, 122.9, 111.5, 108.5, 107.3; IR (ATR-Ge, cm^{-1}): 3309 (phenolic O–H stretch), 3064 (amidic *N*–H stretch), 2824 (carboxylic O–H stretch), 1659 (carbonyl C═O stretch), 1613, 1561, 1516 (aromatic C–C stretch), 1238 (carboxylic C–O stretch), 909 (carboxylic O–H bend).; Elemental analysis: calculated for $C_{13}H_{10}N_2O_4$ (MW 258.23) 60.47% C; 3.90% H; 10.85% N; found: 60.11% C; 3.88% H; 10.47% N; CAS Registry Number 32477-06-8.

3.3.19. ***2-Hydroxy-4-(4-methoxypicolinamido)benzoic acid (3c)***

White solid; Yield 37%; ^{1}H NMR (500 MHz, DMSO-d_6) δ 10.74 (s, 1H), 8.54 (d, J = 5.7 Hz, 1H), 7.74 (d, J = 8.7 Hz, 1H), 7.65 (d, J = 2.6 Hz, 1H), 7.60 (d, J = 2.1 Hz, 1H), 7.54 (d, J = 1.2 Hz, 1H), 7.41 (dd, J = 8.7, 2.1 Hz, 1H), 7.23 (dd, J = 5.7, 2.6 Hz, 1H), 3.93 (s, 4H); ^{13}C NMR (126 MHz, DMSO-d_6) δ 171.9, 166.9, 162.9, 162.3, 151.7, 150.1, 144.2, 134.7, 130.9, 119.9, 113.3, 110.9, 109.9, 108.5, 107.2, 55.9; IR (ATR-Ge, cm^{-1}): 3332 (phenolic O–H stretch), 3079 (amidic *N*–H stretch), 2828 (carboxylic O–H stretch), 1671 (carbonyl C═O stretch), 1653, 1621, 1596 (aromatic C–C stretch), 1232 (carboxylic C–O stretch), 914 (carboxylic O–H bend); Elemental analysis: calculated for $C_{14}H_{12}N_2O_5$ (MW 288.26): 58.33% C; 4.20% H; 9.72% N; found: 57.97% C; 4.17% H; 9.66% N.

3.3.20. ***2-Hydroxy-4-(2-methylisonicotinamido)benzoic acid (4c)***

White solid; Yield 43%; ^{1}H NMR (500 MHz, DMSO-d_6) δ 10.64 (s, 1H), 8.64 (d, J = 5.1 Hz, 1H), 7.77 (d, J = 8.7 Hz, 1H), 7.72 (s, 1H), 7.64 (d, J = 5.1 Hz, 1H), 7.51 (d, J = 2.0 Hz, 1H), 7.31 (dd, J = 8.7, 2.0 Hz, 1H), 2.57 (s, 3H); ^{13}C NMR (126 MHz, DMSO-d_6) δ 171.8, 165.1, 162.1, 158.9, 149.7, 145.2, 142.2, 131.2, 121.2, 119.0, 111.4, 108.7, 107.4, 24.3; IR (ATR-Ge, cm^{-1}): 3320 (phenolic O–H stretch), 3060 (amidic *N*–H stretch), 2821 (carboxylic O–H stretch), 1670 (carbonyl C═O stretch), 1633, 1601, 1569 (aromatic C–C stretch), 1232 (carboxylic C–O stretch), 914 (carboxylic O–H bend); Elemental analysis: calculated for $C_{14}H_{12}N_2O_4$ (MW 272.26): 61.76% C; 4.44% H; 10.20% N; found: 61.59%; 4.24% H; 10.14% N; CAS Registry Number 1978899-28-3.

3.3.21. ***4-(6-Chloronicotinamido)-2-hydroxybenzoic acid (5c)***

White solid; Yield 80%; ^{1}H NMR (500 MHz, DMSO-d_6) δ 10.67 (s, 1H), 8.95–8.91 (m, 1H), 8.34 (dd, J = 8.3, 2.5 Hz, 1H), 7.78 (d, J = 8.7 Hz, 1H), 7.71 (d, J = 8.3 Hz, 1H), 7.50 (d, J = 2.0 Hz, 1H), 7.29 (dd, J = 8.7, 2.0 Hz, 1H); ^{13}C NMR (126 MHz, DMSO-d_6) δ 171.7, 163.7, 162.1, 153.2, 149.7, 145.2, 140.6, 139.4, 131.2, 129.9, 124.7, 124.4, 111.3, 108.8, 107.3; IR (ATR-Ge, cm^{-1}): 3344 (phenolic O–H stretch), 3094 (amidic *N*–H stretch), 2830 (carboxylic O–H stretch), 1674 (carbonyl C═O stretch), 1663, 1632, 1580 (aromatic C–C stretch), 1230 (carboxylic C–O stretch), 915 (carboxylic O–H bend); Elemental analysis: calculated for $C_{13}H_9ClN_2O_4$ (MW 292.68) 53.35% C; 3.10% H; 9.57% N; found: 53.14% C; 3.01% H; 9.54% N; CAS Registry Number 1094765-43-1. **Dihydrate sodium salt of 5c**. Elemental analysis: calculated for $C_{13}H_{12}ClN_2NaO_6$ (MW 350.69) 44.52% C; 3.45% H; 7.99% N; found 44.45% C, 3.40% H; 7.95% N; HPLC purity> 95%.

3.3.22. ***4-(6-Chloropicolinamido)-2-hydroxybenzoic acid (6c)***

White solid; Yield 46%; ^{1}H NMR (600 MHz, DMSO-d_6) δ 10.59 (s, 1H), 8.08 (d, J = 1.5 Hz, 1H), 8.07 (s, 1H), 7.79–7.71 (m, 2H), 7.59 (d, J = 2.0 Hz, 1H), 7.40 (dd, J = 8.7, 2.0 Hz, 1H); ^{13}C NMR (151 MHz, DMSO-d_6) δ 172.1, 162.6, 162.4, 151.1, 149.8, 144.9, 142.1, 131.8, 128.4, 122.6, 112.1, 109.1, 108.0; IR (ATR-Ge, cm^{-1}): 3329 (phenolic O–H stretch), 3061 (amidic *N*–H stretch), 2818 (carboxylic O–H stretch), 1674 (carbonyl C═O stretch), 1641, 1611, 1566 (aromatic C–C stretch), 1247 (carboxylic C–O stretch), 915 (carboxylic O–H bend); Elemental analysis: calculated for $C_{13}H_9ClN_2O_4$ (MW 292.68): 53.35% C; 3.10% H; 9.57% N; 52.12% C; 3.04% H; 9.23% N. CAS Registry Number 1455270-32-2.

3.3.23. ***2-Hydroxy-4-(6-(trifluoromethyl)picolinamido)benzoic acid (7c)***

Beige solid; Yield 41%; ^{1}H NMR (600 MHz, DMSO-d_6) δ 11.33 (s, 1H), 10.95 (s, 1H), 9.09–9.04 (m, 1H), 8.45 (dd, J = 8.3, 2.3 Hz, 1H),

8.30 (d, $J = 8.3$ Hz, 1H), 7.73 (d, $J = 8.7$ Hz, 1H), 7.61 (d, $J = 2.0$ Hz, 1H), 7.46 (dd, $J = 8.7$, 2.0 Hz, 1H); ^{13}C NMR (151 MHz, DMSO-d_6) δ 172.1, 162.6, 162.4, 153.6, 145.9 (q, $J = 4.0$ Hz), 144.9, 136.4 (q, $J = 3.6$ Hz), 131.4, 128.2 (q, $J = 32.5$ Hz), 123.9 (q, $J = 273.0$ Hz), 123.6, 112.0, 109.2, 108.0; IR (ATR-Ge, cm^{-1}): 3345 (phenolic O–H stretch), 3100 (amidic *N*–H stretch), 2841 (carboxylic O–H stretch), 1685 (carbonyl C═O stretch), 1669, 1655, 1601 (aromatic C–C stretch), 1240 (carboxylic C–O stretch), 915 (carboxylic O–H bend). Elemental analysis: calculated for $C_{14}H_9F_3N_2O_4$ (MW 326.05): 51.54% C; 2.78% H; 8.59% N.

3.3.24. 2-Hydroxy-4-(2-hydroxy-6-methylisonicotinamido)benzoic acid (8c)

Beige solid; Yield 27%; ^{1}H- NMR (500 MHz, DMSO-d_6) δ 11.38 (s, 1H), 10.50 (s, 1H), 7.75 (d, $J = 8.7$ Hz, 1H), 7.47 (d, $J = 2.1$ Hz, 1H), 7.29 (dd, $J = 8.7$, 2.1 Hz, 1H), 6.65 (d, $J = 1.8$ Hz, 1H), 2.23 (s, 3H);^{13}C NMR (126 MHz, DMSO) δ 170.2, 165.0, 164.4, 156.6, 150.1, 143.7, 142.9, 132.5, 115.7, 112.3, 108.6, 106.7, 102.9, 23.7; IR (ATR-Ge, cm^{-1}): 3322 (phenolic O–H stretch), 3061 (amidic *N*–H stretch), 2814 (carboxylic O–H stretch), 1661 (carbonyl C═O stretch), 1613, 1587, 1564 (aromatic C–C stretch), 1229 (carboxylic C–O stretch), 911 (carboxylic O–H bend); Elemental analysis: calculated for $C_{14}H_{12}N_2O_5$ (MW 288.26): 58.33% C; 4.20% H; 9.72% N; found: 58.25% C; 4.15% H; 9.37% N.

3.3.25. 4-(2-Chloro-6-methylisonicotinamido)-2-hydroxybenzoic acid (9c)

Beige solid; Yield 39%; ^{1}H NMR (600 MHz, DMSO-d_6) δ 10.64 (s, 1H), 7.76–7.71 (m, 2H), 7.68 (s, 1H), 7.44 (d, $J = 2.1$ Hz, 1H), 7.27–7.22 (m, 1H), 2.46 (s, 3H); ^{13}C NMR (151 MHz, DMSO-d_6) δ 172.1, 163.9, 162.5, 160.7, 150.4, 145.9, 145.2, 131.5, 121.2, 119.8, 111.7, 109.5, 107.8, 24.2; IR (ATR-Ge, cm^{-1}): 3312 (phenolic O–H stretch), 3064 (amidic *N*–H stretch), 2824 (carboxylic O–H stretch), 1670 (carbonyl C═O stretch), 1655, 1612, 1561 (aromatic C–C stretch), 1232 (carboxylic C–O stretch), 914 (carboxylic O–H bend); Elemental analysis: calculated for $C_{14}H_{11}ClN_2O_4$ (MW 306.70): 54.83% C; 3.62% H; 9.13% N; found: 54.60% C; 3.63% H; 9.01% N; CAS Registry Number 1963200-34-1.

3.3.26. 2-Hydroxy-4-(quinoline-2-carboxamido)benzoic acid (10c)

White solid; Yield 93%; ^{1}H NMR (500 MHz, DMSO-d_6) δ 10.84 (s, 1H), 8.70 (t, $J = 1.2$ Hz, 1H), 8.63 (d, $J = 8.4$ Hz, 1H), 8.26 (dd, $J = 8.4$, 1.2 Hz, 1H), 8.24 (d, $J = 8.4$ Hz, 1H), 8.12 (dd, $J = 8.4$, 1.2 Hz, 1H), 7.92 (dd, $J = 8.4$, 6.9 Hz, 1H), 7.79 (d, $J = 8.4$ Hz, 1H), 7.76 (ddd, $J = 8.4$, 6.9, 1.2 Hz, 1H), 7.63 (d, $J = 2.0$ Hz, 1H), 7.51 (d, $J = 1.2$ Hz, 1H), 7.43 (dd, $J = 8.4$, 2.0 Hz, 1H); ^{13}C NMR (126 MHz, DMSO-d_6) δ 172.0, 163.3, 162.5, 149.9, 146.0, 143.8, 138.5, 134.7, 130.9, 130.9, 129.6, 129.2, 128.7, 128.3, 120.1, 118.9, 110.9, 110.7, 107.2; IR (ATR-Ge, cm^{-1}): 3325 (phenolic O–H stretch), 3065 (amidic *N*–H stretch), 2808 (carboxylic O–H stretch), 1688 (carbonyl C═O stretch), 1663, 1620, 1564 (aromatic C–C stretch), 1222 (carboxylic C–O stretch), 912 (carboxylic O–H bend); Elemental analysis: calculated for $C_{17}H_{12}N_2O_4$ (MW 308.29): 66.23% C; 3.92% H; 9.09% N; found: 66.14% C; 3.68% H; 9.00% N. HPLC purity 99.3%. **Sodium salt of 10c.** Elemental analysis: Calculated for $C_{17}H_{11}N_2NaO_4$ (MW 330.27): 61.82%; 3.36% H; 8.48% N; found 61.80% C, 3.30% H; 8.98% N; HPLC purity >95%.

3.3.27. N-(4-oxo-4H-benzo[d] [1,3]dioxin-7-yl)quinoline-2-carboxamide (10c′)

White solid; Yield 73%; ^{1}H NMR (600 MHz, DMSO-d_6) δ 11.14 (s, 1H), 8.60 (d, $J = 8.5$ Hz, 1H), 8.24 (d, $J = 8.5$ Hz, 1H), 8.20 (d, $J = 8.5$ Hz, 1H), 8.09 (d, $J = 8.0$ Hz, 1H), 7.92–7.86 (m, 3H), 7.80 (dd, $J = 8.5$, 2.0 Hz, 1H), 7.73 (t, $J = 7.5$ Hz, 1H), 5.81 (s, 2H); ^{13}C NMR (151 MHz, DMSO-d_6) δ 164.2, 161.4, 159.5, 149.9, 146.4, 146.0, 138.9, 131.4, 131.2, 129.9, 129.6, 129.2, 128.7, 119.4, 116.0, 110.3, 107.1, 91.6; IR (ATR-Ge, cm^{-1}): 3162 (amidic *N*–H stretch), 1781 (carbonyl C═O stretch), 1661, 1641, 1595 (aromatic C–C stretch), 1261 (carboxylic C–O stretch); Elemental analysis: calculated for $C_{18}H_{12}N_2O_4$ (MW 320.30): 67.50% C; 3.78% H; 8.75% N; found: 67.42% C; 3.62% H; 8.45% N. HPLC purity 99.0%

3.3.28. 4-(Picolinamido)benzoic acid (2d)

White solid; Yield 82%; ^{1}H NMR (500 MHz, DMSO-d_6) δ 10.91 (s, 1H), 8.79–8.73 (m, 1H), 8.21–8.14 (m, 1H), 8.09 (td, $J = 7.7$, 1.5 Hz, 1H), 8.07–8.02 (m, 2H), 7.97–7.90 (m, 2H), 7.73–7.68 (m, 1H), 7.67 (d, $J = 1.5$ Hz, 1H); ^{13}C NMR (126 MHz, DMSO-d_6) δ 167.1, 163.1, 149.7, 148.6, 142.6, 138.5, 134.3, 130.4, 127.4, 126.1, 122.9, 119.8, 119.4; IR (ATR-Ge, cm^{-1}): 3210 (amidic *N*–H stretch), 2971 (carboxylic O–H stretch), 1752 (carbonyl C═O stretch), 1622, 1545, 1520 (aromatic C–C stretch), 1288 (carboxylic C–O stretch), 926 (carboxylic O–H bend). ^{1}H NMR (600 MHz, DMSO-d_6) δ 12.75 (bs, 1H, carboxy), 10.95 (s, 1H, amide), 9.27 (s, 1H, aromatic), 8.92–8.89 (m, 1H, aromatic), 8.78 (s, 1H, aromatic), 8.00 (d, $J = 8.4$ Hz, 2H, aromatic), 7.91 (d, $J = 8.4$ Hz, 1H, aromatic); Elemental analysis: calculated for $C_{13}H_{10}N_2O_3$ (MW 242.23): 64.46% C; 4.16% H; 11.56% N; found: 64.26% C; 4.01% H; 11.17% N; CAS Registry Number 5693-36-7.

3.3.29. 4-(6-Chloronicotinamido)benzoic acid (5d)

White solid; Yield 18%; ^{1}H NMR (500 MHz, DMSO-d_6) δ 12.77 (s, 1H), 10.73 (s, 1H), 8.95 (dd, $J = 2.5$, 0.8 Hz, 1H), 8.35 (dd, $J = 8.3$, 2.5 Hz, 1H), 7.99–7.91 (m, 2H), 7.94–7.85 (m, 2H), 7.71 (dd, $J = 8.3$, 0.8 Hz, 1H); ^{13}C NMR (126 MHz, DMSO-d_6) δ 167.1, 163.5, 153.2, 149.6, 142.9, 139.4, 130.5, 129.9, 126.2, 124.3, 119.8; IR (ATR-Ge, cm^{-1}): 3212 (amidic *N*–H stretch), 2976 (carboxylic O–H stretch), 1756 (carbonyl C═O stretch), 1624, 1542, 1523 (aromatic C–C stretch), 1274 (carboxylic C–O stretch), 925 (carboxylic O–H bend); Elemental analysis: calculated for $C_{13}H_9ClN_2O_3$ (MW 276.68): 56.44% C; H, 3.28% H; 10.13% N; found: 56.33% C; 3.15% H; 10.00% N; CAS Registry Number 1053982-70-9.

3.3.30. 4-(6-Chloropicolinamido)benzoic acid (6d)

White solid; Yield 26%; ^{1}H NMR (600 MHz, DMSO-d_6) δ 12.77 (s, 1H), 10.66 (s, 1H), 8.12–8.04 (m, 2H), 8.01–7.95 (m, 2H), 7.93–7.88 (m, 2H), 7.80–7.74 (m, 1H); ^{13}C NMR (151 MHz, DMSO-d_6) δ 167.4, 162.4, 151.2, 149.8, 142.7, 142.1, 130.7, 128.4, 126.6, 122.6, 120.5; IR (ATR-Ge, cm^{-1}): 3214 (amidic *N*–H stretch), 2975 (carboxylic O–H stretch), 1756 (carbonyl C═O stretch), 1651, 1602, 1580 (aromatic C–C stretch), 1278 (carboxylic C–O stretch), 918 (carboxylic O–H bend); Elemental analysis: calculated for $C_{13}H_9ClN_2O_3$ (MW 276.68): 56.44% C; 3.28% H; 10.13% N; found: 56.27% C; 3.16% H; 9.87% N; CAS Registry Number 1275816-32-4.

3.3.31. 4-(6-(Trifluoromethyl)picolinamido)benzoic acid (7d)

Beige solid; Yield 42%; M. p. 227–228 °C; ^{1}H NMR (500 MHz, DMSO-d_6) δ 13.17 (s, 1H), 9.11–9.07 (m, 1H), 8.39 (ddd, $J = 8.2$, 2.4, 0.8 Hz, 1H), 8.21 (dt, $J = 8.2$, 0.8 Hz, 1H), 7.99–7.90 (m, 2H), 7.64–7.57 (m, 1H), 7.54–7.44 (m, 2H); ^{13}C NMR (126 MHz, DMSO) δ 167.8, 165.6, 152.5, 146.7 (d, $J = 4.0$ Hz), 135.7 (q, $J = 3.6$ Hz), 133.3, 131.2, 127.9 (q, $J = 32.5$ Hz), 123.8 (q, $J = 273.0$ Hz); IR (ATR-Ge, cm^{-1}): 3350 (amidic *N*–H stretch), 2994 (carboxylic O–H stretch), 1762 (carbonyl C═O stretch), 1674, 1641, 1599 (aromatic C–C stretch), 1294 (carboxylic C–O stretch), 915 (carboxylic O–H bend); Elemental analysis: calculated for $C_{14}H_9F_3N_2O_3$ (MW 310.23): 54.20% C; 2.92% H; 9.03% N; CAS Registry Number 2464470-66-2.

3.3.32. 4-(Quinoline-2-carboxamido)benzoic acid (10d)

White solid; Yield 59%; M. p. 232–233 °C; ^{1}H NMR (500 MHz, DMSO-d_6) δ 12.84 (s, 1H), 11.00 (s, 1H), 8.63 (d, $J = 8.2$ Hz, 1H), 8.31–8.21 (m, 2H), 8.14–8.05 (m, 3H), 8.02–7.95 (m, 2H), 7.92 (ddd, $J = 8.2$, 6.8, 1.5 Hz, 1H), 7.76 (ddd, $J = 8.2$, 6.8, 1.5 Hz, 1H); ^{13}C NMR (126 MHz, DMSO-d_6) δ 167.1, 163.3, 149.9, 146.1, 142.5, 138.5, 130.9, 130.5, 129.5, 129.2, 128.7, 128.3, 126.1, 119.8, 118.9; IR (ATR-Ge,

cm^{-1}): 3214 (amidic *N*–H stretch), 2977 (carboxylic O–H stretch), 1762 (carbonyl C═O stretch), 1602, 1574, 1515 (aromatic C–C stretch), 1267 (carboxylic C–O stretch), 920 (carboxylic O–H bend); Elemental analysis: calculated for $C_{17}H_{12}N_2O_3$ (MW 292.29): 69.86% C; 4.14% H; 9.58% N; found: 69.69% C; 4.04% H; 9.23% N. CAS Registry Number 190437-68-4.

3.3.33. Picolinamide

White solid; Yield 89%; M. p. 59–61 °C; ^{1}H NMR (500 MHz, DMSO-d_6) δ 8.62 (ddd, J = 4.8, 1.7, 0.9 Hz, 1H), 8.12 (s, 1H), 8.03 (dt, J = 7.7, 1.2 Hz, 1H), 7.97 (td, J = 7.7, 1.7 Hz, 1H), 7.68–7.63 (m, 1H), 7.58 (ddd, J = 7.5, 4.8, 1.2 Hz, 1H); ^{13}C NMR (126 MHz, DMSO-d_6) δ 166.5, 150.8, 148.9, 138.1, 126.9, 122.4, 39.5; IR (ATR-Ge, cm^{-1}): 3014 (amidic *N*–H stretch), 1746 (carbonyl C═O stretch), 1631, 1599, 1540 (aromatic C–C stretch), 1212 (carboxylic C–O stretch); Elemental analysis: calculated for $C_6H_6N_2O$ (122.13) 59.01% C; 4.95% H; 22.94% N; found 58.92% C; 4.90% H; 22.87% N; CAS Registry Number 1452-62-6.

3.3.34. Quinoline-2-carboxamide

White solid; Yield 90%; M. p. 78–80 °C; ^{1}H NMR (500 MHz, DMSO-d_6) δ 8.54 (dd, J = 8.5, 1.0 Hz, 1H), 8.29 (s, 1H), 8.15 (d, J = 8.5 Hz, 1H), 8.11 (d, J = 8.5, 1.0 Hz, 1H), 8.06 (d, J = 8.2, 1.5 Hz, 1H), 7.85 (ddd, J = 8.5, 6.8, 1.5 Hz, 1H), 7.80–7.77 (m, 1H), 7.70 (ddd, J = 8.2, 6.8, 1.0 Hz, 1H); ^{13}C NMR (126 MHz, DMSO-d_6) δ 165.2, 157.9, 150.1, 136.1, 130.6, 130.1, 129.4, 127.6, 127.0, 119.2; IR (ATR-Ge, cm^{-1}): 3022 (amidic *N*–H stretch), 1751 (carbonyl C═O stretch), 1641, 1577, 1523 (aromatic C–C stretch), 1210 (carboxylic C–O stretch); Elemental analysis: calculated for $C_{10}H_8N_2O$ (172.19) 69.76% C; 4.68% H; 16.27% N; found 69.70% C; 4.60% H; 16.22% N. CAS Registry Number 5382-42-3.

3.3.35. 4-Methoxypicolinamide

Beige solid; Yield 75%; M. p. 99–100 °C; ^{1}H NMR (600 MHz, DMSO-d_6) δ 8.40 (d, J = 5.5 Hz, 1H), 8.04 (s, 1H), 7.61 (s, 1H), 7.51 (d, J = 2.7 Hz, 1H), 7.10 (dd, J = 5.6, 2.7 Hz, 1H), 3.85 (s, 3H); ^{13}C NMR (126 MHz, DMSO-d_6) δ165.2, 159.6, 152.3, 146.7, 112.0, 106.9, 55.9; IR (ATR-Ge, cm^{-1}): 3025 (amidic *N*–H stretch), 1751 (carbonyl C═O stretch), 1641, 1602, 1570 (aromatic C–C stretch), 1211 (carboxylic C–O stretch); Elemental analysis: calculated for $C_7H_8N_2O_2$ (152.15) 55.26% C; 5.30% H; 18.41% N; found 55.18% C; 5.30% H; 18.33% N; CAS Registry Number 9014-93-1.

4. Conclusion

As an attempt to prepare new, potentially active antimycobacterials, we designed a number of pyridine carboxamides, subdivided into two series; (I) pyridine carboxylic acids linked to aminopyrazine or 6-chloropyrazin-2-amine (the rationale is to combine fragments from isoniazid and pyrazinamide); (II) pyridine carboxylic acids linked to 4-aminosalicylic acid or 4-aminobenzoic acid (the rationale is to combine fragments from isoniazid and 4-aminosalicylic acid). Several structural modifications were attempted in order to study structure-activity relationships. *In vitro* antimycobacterial results showed the superiority of series (II) over (I) and the superiority of 4-aminosalicylic acid over 4-aminobenzoic acid in series (II). It was also shown that forming the δ-lactone of 4-aminosalicylic acid as an attempt to enhance mycobacterial cell wall penetration retained antimycobacterial activity. Compound **10c**, bearing quinaldic acid linked to 4-aminosalicylic acid, was the most promising compound as it preserved its potent *in vitro* antimycobacterial activity also against multidrug-resistant *Mtb* strains. Furthermore, compound **10c** had no cytotoxicity *in vitro* nor *in vivo* when tested in the *Galleria mellonella* model. Compound **10c** was found to significantly reduce CFU in the spleens of the murine model of tuberculosis. Biochemical studies with mutants overexpressing enzymes of the folate pathways did not confirm this mechanism of action. Nevertheless, compound **10c** affected the production of lipids and mycolic acids in mycobacteria and affected methionine metabolism possibly by affecting either the activity of methyltransferases or the level of *S*-adenosylmethionine in mycobacteria. *In silico* simulations based on molecular docking and subsequent MD assessment of the stability of acquired poses concluded the possibility of binding to mycobacterial Met-tRNA synthetase (mtMetRS).

Metabolic study in human liver microsomes showed that compound **10c** is metabolized by slow hydrolysis of the amidic bond to yield quinaldic acid and 4-aminosalicylic acid (both of which are nontoxic) with a half-life of 630 min which is significantly longer than PAS half-life. On the other hand, the lactone **10c′** was quickly hydrolyzed to the open form, compound **10c**, with half-life of 11 min. Therefore, we propose compound **10c** and its lactone **10c′** as two promising antitubercular agents that solve the issues of the short half-life of PAS and toxic formation of hydrazine metabolite of INH, while preserving potent *in vitro*/*in vivo* antimycobacterial activity.

Authors contribution

D.E.N., G.B., J.Z. and M.D. designed the study; D.E.N. and G.B. synthesized final compounds; D.E.N. and G.B. interpreted analytical data and results of biological screening; O.J., K.K., and P.P. performed biological screening (antimycobacterial, antibacterial, antifungal); K.K. performed *in vivo* toxicity screening in *Galleria mellonella*. P.B. performed *in vitro* cytotoxicity screening and interpreted its results; M.N. and R.K. performed metabolic study; J. Ze., M.F., and J.K. performed mechanism of action study; O.P. and P.K. performed *in vivo* screening in murine model of TB; J.Z. performed *in silico* studies. All authors contributed equally to writing the final draft of the manuscript. All authors read and approved the final draft of the manuscript.

Funding

This work was supported by EFSA-CDN (No. CZ.02.1.01/0.0/0.0/16_019/0000841) co-funded by ERDF (grant to G.B. and M.D.). J.Z. acknowledges the support of "The project National Institute of virology and bacteriology (Programme EXCELES, ID Project No. LX22NPO5103) - Funded by the European Union - Next Generation EU." Supported by Ministry of Health of the Czech Republic, grant no. NU21-05-00482 (grant to J.Z.). This study was partially supported by MH CZ-DRO (University Hospital Hradec Kralove, Nr. 00179 906), by Charles University, Czech Republic (Nr. SVV 260 666), by Slovak Research and Development Agency (grant n. APVV-19-0189), and by the OPII, ACCORD, ITMS2014+: 313021X329, co-financed by ERDF.

Declaration of competing interest

The authors declare that they have no known competing financial interests or personal relationships that could have appeared to influence the work reported in this paper.

Data availability

No data was used for the research described in the article.

Acknowledgement

We would like to thank Natália Kotríková from Comenius University in Bratislava for technical help with preparation of the constructs used in the study, Jana Vacková and Ida Dufková for help with basic microbiological screening. Computational resources were supplied by the project "e-Infrastruktura CZ" (e-INFRA CZ LM2018140) supported by the Ministry of Education, Youth and Sports of the Czech Republic.

Appendix A. Supplementary data

Supplementary data to this article can be found online at https://doi.org/10.1016/j.ejmech.2023.115617.

References

[1] World Health Organization, WHO Consolidated Guidelines on Tuberculosis. Module 5: Management of Tuberculosis in Children and Adolescents, 2022. Geneva.
[2] S.A.A. Abdel-Raheem, et al., Facile synthesis and pesticidal activity of substituted heterocyclic pyridine compounds, Rev. Roum. Chem. 67 (4–5) (2022) 305–309.
[3] V.W.L. Ng, et al., Antimicrobial polycarbonates: investigating the impact of nitrogen-containing heterocycles as quaternizing agents, Macromolecules 47 (4) (2014) 1285–1291.
[4] M.M. Heravi, V. Zadsirjan, Prescribed drugs containing nitrogen heterocycles: an overview, RSC Adv. 10 (72) (2020) 44247–44311.
[5] F.G. Winder, P. Collins, S.A. Rooney, Effects of isoniazid on mycolic acid synthesis in Mycobacterium tuberculosis and on its cell envelope, Biochem. J. 117 (2) (1970) 27P.
[6] P. Gopal, et al., Pharmacological and molecular mechanisms behind the sterilizing activity of pyrazinamide, Trends Pharmacol. Sci. 40 (12) (2019) 930–940.
[7] S. Chakraborty, et al., Para-aminosalicylic acid acts as an alternative substrate of folate metabolism in Mycobacterium tuberculosis, Science 339 (6115) (2013) 88–91.
[8] P. Wang, et al., Isoniazid metabolism and hepatotoxicity, Acta Pharm. Sin. B 6 (5) (2016) 384–392.
[9] Para-aminosalicylic acid, Tuberculosis 88 (2) (2008) 137–138.
[10] F. Lin, et al., A catalyst-free, facile and efficient approach to cyclic esters: synthesis of 4H-benzo[d][1,3]dioxin-4-ones, RSC Adv. 4 (38) (2014) 19856–19860.
[11] B.K.M. Murali, B. Iyer, M. Sirsi, p-Pyridoylaminobenzoic acids and their derivatives as possible tuberculostats, J. Indian Inst. Sci. 51 (3) (1969) 285–304.
[12] D.S. Goldfarb, Method for Altering the Lifespan of Eukaryotic Organisms, 2008 (US8642660B2).
[13] S.X. Cai, J.A. Drewe, Substituted Nicotinamides and Analogs as Activators of Caspases and Inducers of Apoptosis and the Use Thereof, 2002 (US7041685B2).
[14] Y.P.T. Pang, E. N, C.B. Millard, Small-molecule Inhibitors of Protein Synthesis Inactivating Toxins, 2009 (US20110263540).
[15] S.Y. Kim, et al., Pharmacophore-based virtual screening: the discovery of novel methionyl-tRNA synthetase inhibitors, Bioorg. Med. Chem. Lett 16 (18) (2006) 4898–4907.
[16] G. Bouz, J. Zitko, Inhibitors of aminoacyl-tRNA synthetases as antimycobacterial compounds: an up-to-date review, Bioorg. Chem. (2021) 110.
[17] S.G. Franzblau, et al., Rapid, low-technology MIC determination with clinical Mycobacterium tuberculosis isolates by using the microplate Alamar Blue assay, J. Clin. Microbiol. 36 (2) (1998) 362–366.
[18] M.T. Heinrichs, et al., Mycobacterium tuberculosis strains H37ra and H37rv have equivalent minimum inhibitory concentrations to most antituberculosis drugs, International Journal of Mycobacteriology 7 (2) (2018) 156–161.
[19] C.H. Hsiao, T.F. Tsai, P.R. Hsueh, Characteristics of skin and soft tissue infection caused by non-tuberculous mycobacteria in Taiwan, Int. J. Tubercul. Lung Dis. 15 (6) (2011) 811–817.
[20] S.L. Kordus, et al., Mechanism of selectivity reveals novel antifolate drug interactions, bioRxiv (2020), 2020.09.18.304022.
[21] C.H. Lee, H.S. Lee, Growth inhibiting activity of quinaldic acid isolated from ephedra pachyclada against intestinal bacteria, Journal of the Korean Society for Applied Biological Chemistry 52 (4) (2009) 331–335.
[22] S. Shenoi, et al., Multidrug-resistant and extensively drug-resistant tuberculosis: consequences for the global HIV community, Curr. Opin. Infect. Dis. 22 (1) (2009) 11–17.
[23] European Committee for Antimicrobial Susceptibility Testing (EUCAST) of the European Society of Clinical Microbiology and Infectious Diseases (ESCMID), Determination of Minimum Inhibitory Concentrations (MICs) of Antibacterial Agents by Broth Dilution, 2003, pp. 1–7.
[24] M.C.M. Arendrup, J, J.W. Mouton, K. Lagrou, P. Hamal, J. Guinea, Subcommittee on antifungal susceptibility testing (AFST) of the ESCMID European committee for antimicrobial susceptibility testing (EUCAST), *Method for the Determination of broth dilution minimum inhibitory Concentrations of Antifungal agents for yeasts*, in: EUCAST Definitive Document E.Def 7.*3.1*. 2017, 2017.
[25] M.C.M. Arendrup, J, J.W. Mouton, K. Lagrou, P. Hamal, J. Guinea, Subcommittee on antifungal susceptibility testing (AFST) of the ESCMID European committee for antimicrobial susceptibility testing (EUCAST), Method for the Determination of Broth Dilution Minimum Inhibitory Concentrations of Antifungal agents for Conidia Forming Moulds (2017).
[26] K. Ignasiak, A. Maxwell, Galleria mellonella (greater wax moth) larvae as a model for antibiotic susceptibility testing and acute toxicity trials, BMC Res. Notes 10 (1) (2017) 428.
[27] J. Zheng, et al., para-Aminosalicylic acid is a prodrug targeting dihydrofolate reductase in Mycobacterium tuberculosis (vol 288, pg 23447, 2013), J. Biol. Chem. 288 (40) (2013), 28951-28951.
[28] G. Karabanovich, et al., Development of 3,5-dinitrophenyl-containing 1,2,4-triazoles and their trifluoromethyl analogues as highly efficient antitubercular agents inhibiting decaprenylphosphoryl-beta-d-ribofuranose 2'-oxidase, J. Med. Chem. 62 (17) (2019) 8115–8139.
[29] J.O. Kilburn, K. Takayama, Effects of ethambutol on accumulation and secretion of trehalose mycolates and free mycolic acid in Mycobacterium smegmatis, Antimicrob. Agents Chemother. 20 (3) (1981) 401–404.
[30] C. Vilchèze, et al., Inactivation of the inhA-encoded fatty acid synthase II (FASII) enoyl-acyl carrier protein reductase induces accumulation of the FASI end products and cell lysis of Mycobacterium smegmatis, J. Bacteriol. 182 (14) (2000) 4059–4067.
[31] A.E. Grzegorzewicz, et al., A common mechanism of inhibition of the Mycobacterium tuberculosis mycolic acid biosynthetic pathway by isoxyl and thiacetazone, J. Biol. Chem. 287 (46) (2012) 38434–38441.
[32] B. Hajian, et al., Drugging the folate pathway in Mycobacterium tuberculosis: the role of multi-targeting agents, Cell Chem. Biol. 26 (6) (2019) 781–791, e6.
[33] Cyprotex, Microsomal stability assay, September 2021]; Available from: https://www.cyprotex.com/admepk/in-vitro-metabolism/microsomal-stability, 2021.
[34] E. Nepovimova, et al., Tacrine-trolox hybrids: a novel class of centrally active, nonhepatotoxic multi-target-directed ligands exerting anticholinesterase and antioxidant activities with low in vivo toxicity, J. Med. Chem. 58 (22) (2015) 8985–9003.